Lawrence Berkeley Laboratory
UNIVERSITY OF CALIFORNIA

Physics Division

Submitted to Annual Review of
Nuclear and Particle Sciences

Particle Composition in Hadronic Jets in e^+e^- Annihilation

W. Hofmann

March 1988

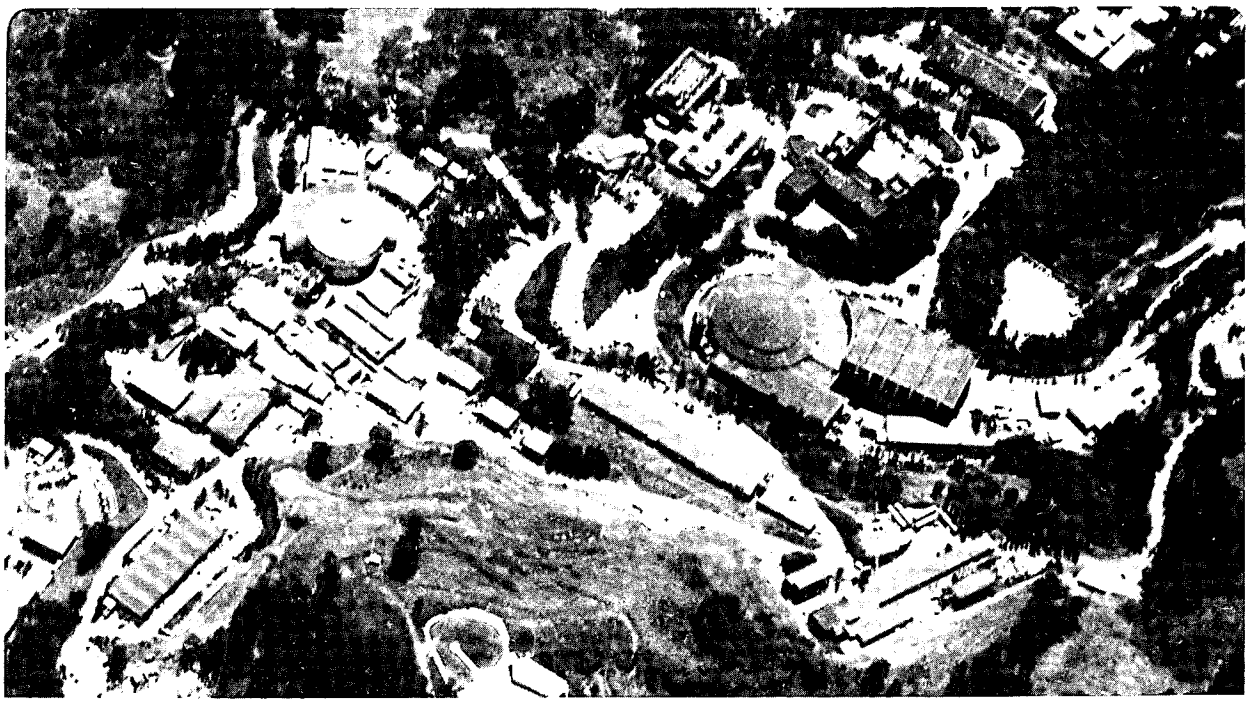

Prepared for the U.S. Department of Energy under Contract DE-AC03-76SF00098

DISCLAIMER

LBL-24897

PARTICLE COMPOSITION IN HADRONIC JETS IN e^+e^- ANNIHILATION

Werner Hofmann

Lawrence Berkeley Laboratory

University of California

Berkeley, CA 94720

March 1988

To be published in

ANNUAL REVIEW OF NUCLEAR AND PARTICLE SCIENCE

This work was supported by the U.S. Department of Energy under Contract No. DE-AC03-76SF00098, and by the Alfred P. Sloan Foundation.

INTRODUCTION

Although Quantum Chromodynamics (QCD) is believed to be the fundamental theory of hadronic processes, there are as yet no prescriptions by which physical hadronic amplitudes for processes such as $e^+e^- \rightarrow q\bar{q} \rightarrow$ hadrons can be calculated. Predictions at the hadron level are either based on phenomenological models to describe parton fragmentation, or refer to general, but somewhat vague ideas like local duality between hadron and parton distributions. Experimental studies of the spectra and composition of particles in hadronic jets are of great relevance in the evolution of the phenomenology, and ultimately in providing guidance to the development of suitable non-perturbative methods. In particular, e^+e^- annihilation into $q\bar{q}$ has the advantage of providing a well-defined initial parton configuration, without involving poorly-known hadronic wave functions. This review summarizes the main results on inclusive spectra and particle composition of hadronic jets in e^+e^- annihilation in the 10-40 GeV energy range.

INCLUSIVE CROSS SECTIONS FOR HADRON PRODUCTION

Fragmentation Functions

In e^+e^- annihilation at a center-of-mass energy $\sqrt{s}$, the inclusive cross section for production of a hadron h of scaled energy (in the cms) $x \equiv 2E/\sqrt{s}$ can be written as

$$\frac{d\sigma}{dx} = \sum_q \frac{4\pi}{s} \alpha^2 e_q^2 (1+\varepsilon) \left(D_q^h(x,s) + D_{\bar{q}}^h(x,s) \right) \qquad (1)$$

The quark fragmentation functions D_q^h are the primary quantities of interest: they describe the rate dn_h/dx of hadrons h produced in the fragmentation of a quark q. The $(1+\varepsilon)$ term represents QCD and electroweak corrections to the total cross section. The D's are expected to scale in x, up to logarithmic corrections. At very low x, phase-space effects require $(d\sigma/dx) \sim \beta = p/E$. Inclusive cross sections are therefore often quoted in the scale-invariant form $(s/\beta)(d\sigma/dx)$. Since we are interested in the number of fragmentation products per

primary quark pair, it is furthermore convenient to normalize production cross sections to the total hadronic cross section σ_{tot}, and to quote $(1/\sigma_{tot}\beta)(d\sigma/dx)$, or briefly $(1/\sigma\beta)(d\sigma/dx)$.

General Formalism

For completeness, we mention the general formalism for inclusive hadron production in the annihilation of (unpolarized) electrons and positrons (neglecting electroweak corrections). Inclusive cross sections depend on the invariant products of four-vectors: $s \equiv (p_{e+} + p_{e-})^2$, $x \equiv 2p_h (p_{e+} + p_{e-})/s = 2E/\sqrt{s}$, and $\{2p_h (p_{e+} - p_{e-})/s\}^2 = \beta^2 x^2 \cos^2\theta$ (with $p_h = (E,\vec{p})$, and $\beta = p/E$). Here θ stands for the polar angle of the hadron in the e^+e^- cms. Traditionally (1), σ is expressed in terms of two structure functions $\overline{W}_1$ and $\overline{W}_2$,

$$\frac{d^2\sigma}{dx d\Omega} = \frac{\alpha^2}{s}\beta x \{m\overline{W}_1(\sqrt{s},\nu) + \frac{1}{4}\beta^2 x \nu \overline{W}_2(\sqrt{s},\nu) \sin^2\theta\} \qquad (2),$$

with $\nu=(E/m)\sqrt{s}$. The structure functions $\overline{W}_1$ and $\overline{W}_2$ are expected to scale:

$$m\overline{W}_1(\sqrt{s},\nu) \rightarrow -\overline{F}_1(x) \quad \text{and} \quad \nu\overline{W}_2(\sqrt{s},\nu) \rightarrow \overline{F}_2(x) \qquad (3).$$

Based on dimensional counting arguments, the F's are predicted to fall like $(1-x)^n$ for $x \rightarrow 1$. The exponent n reflects the number of constituents in the hadron; in particular, we expect $n=2$ for mesons and $n \geq 3$ for baryons (1,2).

Besides x and θ, we will consider kinematic variables defined with respect to the direction of the initial quarks, such as the rapidity $y = \frac{1}{2}\log\left(\frac{E+p_{\parallel}}{E-p_{\parallel}}\right)$ or the transverse momentum p_T of a particle. Of course, the quark direction is experimentally not known, but can be reconstructed from the final-state hadrons with sufficient accuracy (3-5° at $\sqrt{s} \approx 30$ GeV). We shall treat distributions referring to such a jet axis as inclusive cross sections, although, strictly speaking, they represent multi-particle cross sections integrated over most degrees of freedom in a rather nontransparent fashion, and are biased by the choice of the axis (usually the sphericity or thrust axis).

PHENOMENOLOGY OF PARTON FRAGMENTATION

Numerous phenomenological models with widely varying degrees of sophistication have been proposed to predict or to postdict hadron production in e^+e^- annihilation. Several excellent reviews (3-7) cover different facets of the problem; the latest review by Sjöstrand (4) provides an exemplary introduction to current phenomenology and its historical development. In the following, we review the presently favored approaches. Evolved from analytical predecessors, these modern models are formulated in terms of Monte Carlo generators creating exclusive final states, thus allowing a direct comparison with experimental results.

Parton Cascades

Hadron production in e^+e^- annihilation is modeled in several steps (Figure 1). The virtual photon creates a pair of quarks (stage I). These quarks are highly off-shell and cascade down to the mass shell via successive gluon emission, initiating a "quark-gluon shower" (stage II). Since exact matrix elements are only known up to second order in α_s, corresponding to four-parton final states, the evolution of partons is usually described as a branching process (8,9,10) accounting for the leading infrared and collinear terms. Since the triple-gluon coupling is large compared to the quark-gluon coupling, the parton evolution proceeds almost entirely through the $g \rightarrow gg$ process; quark pair production is infrequent. Two parameters characterize the evolution of partons: the QCD scale Λ and the minimum virtuality Q_0, beyond which the evolution is cut off. For typical $Q_0 \approx 1$ GeV and $\Lambda \approx 400$ MeV, an annihilation event at PEP or PETRA energies ($\sqrt{s} \approx 30$-40 GeV) contains on average about three to four gluons in addition to the two initial quarks. The main problem is now to establish the connection between these perturbative partons and the hadrons.

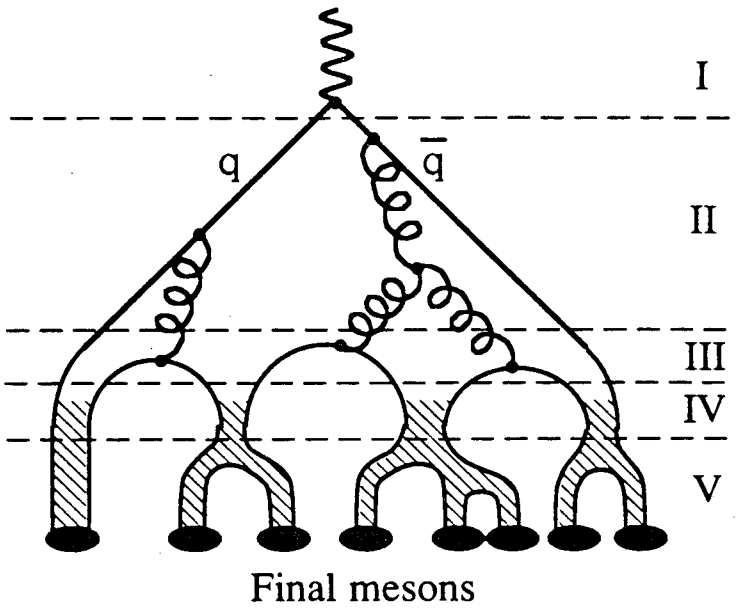

Figure 1 Phenomenological model of hadron production in e^+e^- annihilation, with the stages of (I) formation of the initial quark-antiquark pair, (II) evolution of the parton cascade, (III) conversion of cascade gluons into quark-antiquark pairs, (IV) formation of primary hadronic objects, and (V) decay of these primary hadrons into stable observable particles.

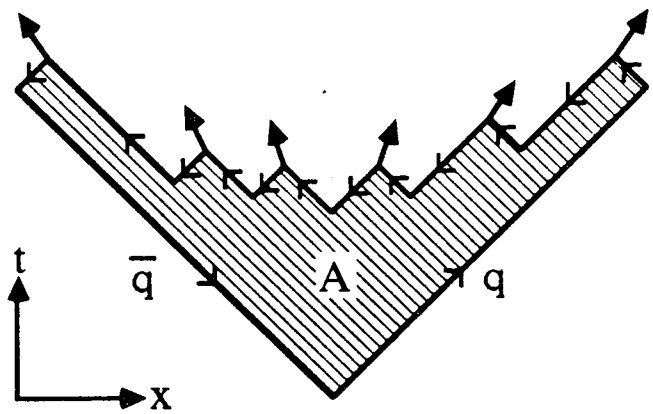

Figure 2 Space-time diagram for particle describing hadron production in the decay of a (one-dimensional) color string. Energy and momentum of a hadron are determined by the space and time difference of the production points of its quarks, multiplied by the string tension κ. A denotes the space-time area enclosed by the primary quark loop (here, antiquarks are represented as quarks moving backward in time).

Local Parton-Hadron Duality

The use of QCD to describe the structure of the final state in e^+e^- annihilation rests on the assumption of a minimum duality between the angular flow of partons and the flow of hadrons. One can carry this duality further and postulate that the momentum distribution of hadrons of mass m reflects the momentum distribution of partons of virtuality $Q \approx m$ in the parton cascade (11). Analytical estimates of the parton distribution based on a modified leading log approximation (11) result in finite parton multiplicities for $Q_0 = \Lambda$ (a consequence of destructive interference between soft gluons) and allow the description even of pion spectra with this method (using $Q_0 = \Lambda \approx m_\pi$). One may argue against such modeling, since most pions stem from resonance decays and have little connection to the parton cascade; on the other hand, hadron decays can be viewed as just another aspect of parton evolution and should be reasonably mocked up by the evolution equations. Along the same lines, one can even speculate about an exclusive duality between multi-gluon and multi-hadron final states (12).

While these applications of parton-hadron duality are certainly intriguing, they are not (yet) able to give detailed predictions for the hadron composition of jets, given that hadronic quantum numbers are completely ignored. Phenomenological fragmentation models therefore incorporate some explicit mechanism to achieve the transition from partons to hadrons.

QCD Cluster Models

Following the shower evolution, one needs to postulate some (nonperturbative) mechanism for the abundant production of new $q\bar{q}$ pairs (Figure 1, stage III), and for the subsequent formation of primary meson-like objects (stage IV). One philosophy, for historical reasons referred to as "QCD cluster models", is to convert gluons from previous

perturbative stage into $q\bar{q}$ pairs. The Webber model (13) as well as the Fox-Wolfram/Field-Wolfram (14,15), and Caltech I (16) models fall into this class. In the limit $N_C \to \infty$, each of these quarks has a well-defined antiquark partner - its neighbor in the tree structure of the event - with which it recombines to form a color singlet (17) (see Figure 1). For sufficiently low Q_0, the mass of those singlets will be in the GeV range. They can be identified either with normal hadrons, or with clusters (excited meson states, somewhat along the lines of Hagedorn's bootstrap model), or with a mixture of both. Finally, these primary objects decay (stage V). Since they are bound $q\bar{q}$ states, all information about initial color field directions is lost and the decay proceeds isotropically.

QCD cluster models have the appealing feature that all ingredients seem well-defined and known: the gluon splitting into $q\bar{q}$ looks like an ordinary QCD process, and a $q\bar{q}$ color singlet of mass M produced in the process should decay in identically the same way as a $q\bar{q}$ pair produced in low-energy e^+e^- annihilation at $\sqrt{s} = M$. The decay properties of such clusters can either be parameterized after low-energy data (18), or be approximated by two-body decay chains governed by the available phase space (13). The hadron composition of the final state follows as a convolution of cluster decay properties with the mass spectrum of clusters. Given that there are (essentially) only two phenomenological parameters, Λ and Q_0, the success of QCD cluster models in reproducing the main features of event topology, inclusive spectra and particle composition is truly remarkable (13,16).

More detailed comparison with experimental data, however, reveals fundamental problems. For example, data on baryon correlations (19,20) can be explained only if one allows for occasional gluon splitting into diquark-antidiquark, clearly going beyond any perturbative description. Furthermore, the experimental inclusive pion spectra at high momentum require that some pions are produced directly, without the intermediate cluster decay (21). Since the models give continuous $q\bar{q}$ mass spectra, an ad-hoc mapping of low-

mass clusters onto meson states is required. In addition, any cluster model faces occasional "pathological" events where no gluons are emitted in the evolution of the initial quarks. These conceptual problems have reduced the popularity of QCD cluster models as a "parameter-free" description of hadronization processes, and many of the initial models have been abandoned.

String Models

Whereas QCD cluster models view the color field at large distances as a collection of (non-interacting) quanta, string models (22,23,24) use the analogy of a classical field (contracted effectively into one dimension due to the non-abelian nature of QCD). Quark and antiquark represent the momentum-carrying ends of this color flux tube, or string. Perturbative gluons are re-interpreted as momentum concentrations, or kinks along the string (24). The energy density κ in the flux tube can be estimated to about 1 GeV/fm. In this field, new $q\bar{q}$ pairs are born and break the string into short segments representing hadrons or clusters (Figure 2). String models and QCD cluster models are dual in the sense that they try to describe the same physical process using orthogonal approximations. It is therefore not completely surprising that the two classes of models exhibit the same space-time structure (the "inside-outside cascade" (3)) and yield closely related patterns of particle flow (25).

No general quantum mechanical treatment of string dynamics is known, not even for the one-dimensional case. In a 1+1 dimensional system, neglecting the quantization of string masses, the rate of creation of a new $q\bar{q}$ pairs per unit string length is constant. The Lorentz-invariant production rate $d\Gamma_n$ of a given configuration of n primary hadrons h_i is hence governed by the space-time area A swept by the string (Figure 2) (24):

$$d\Gamma_n \sim \{\Pi\, N_i\, dp_i\, \delta(p_i^2-m_i^2)\}\, \delta(\Sigma p_i - P)\, \exp(-bA)\, F(h_1 \ldots h_n) \qquad (4).$$

Here the p_i are hadron two-momenta, P is the total energy-momentum of the state, and the N_i and b are phenomenological parameters related to the multiplicity distribution. Clebsch-Gordan coefficients and mixing angles relating quark states to meson states are collected in the factor F. The Caltech II model (21) works in this contiuum limit: relatively few breaks of the string create massive color-singlet clusters with a continuous spectrum.

An opposite extreme is provided by the Lund model (24). There, string fragments are identified with the usual mesons and baryons. The distribution of break points is governed by a rather general symmetry requirement (26). Technically, string fragmentation is implemented as an iterative scheme analogous to the Feynman-Field model (27): one hadron at a time is peeled off the end of the string, carrying a (light-cone) fraction z of the string's energy-momentum. Within the postulates of the model, the distribution f(z) has a unique functional form (26):

$$f(z) = \frac{(1-z)^a}{z} \exp\left(\frac{-bm^2}{z}\right) \qquad (5).$$

Here m stands for the (transverse) mass of the hadron; a and b are free parameters. Of course, the (1-z) term essentially reflects 1-dimensional multi-body phase space, and the exponential term is reminiscent of the area law in Equation (4). To account for production rates of different hadron flavors, the Lund model introduces a slew of new parameters for the frequency with which different quark flavors are produced in the decay of the string, and the frequency with which different hadron spin states are produced. Due to the finite energy density in the string, $\kappa \approx 1$ GeV^2, the creation of heavy quark-antiquark pairs is expected to be exponentially suppressed (28). Production of $J = 0$ hadron states should be favored over $J > 0$ states, due to the higher binding energy of the former (24). However, lacking a true quantum mechanical treatment of the string, it is clear that these arguments are qualitative rather than quantitative, and that details of the particle composition remain a matter of parameterization.

Determination of Model Parameters

While approximate values for most model parameters can be obtained by educated guesses, their precise values are always adjusted for best fit to the experimental data. Since any given hadron spectrum is always sensitive to several parameters, multi-parameter fitting procedures have been developed which simultaneously adjust several parameters to fit a comprehensive selection of experimental distributions, and derive error limits. However, since no model is perfect, the results of such fits tend to depend quite a bit on the selection of data sets, and on the relative weight given to different distributions.

Another problem is related to heavy (charm and bottom) quark production. Decays of charm and bottom hadrons contribute a substantial fraction of the observed hadrons in e^+e^- annihilation (Table 1). Unfortunately, for most species of heavy hadrons neither their production rates nor their decay modes are known. Incomplete modeling of these contributions or failure to consider the associated uncertainties can result in significant differences in the fragmentation parameters for ordinary quarks, as pointed out in (29), (30), and (31). In the Lund model, e.g., it appears that the number of ϕ's from charm and bottom decays is overestimated (31).

Table 1: Fraction of hadrons from resulting from decays of heavy (charm and bottom) hadrons, based on Lund model.

π	21%	ρ	10%	p	8%
K	35%	K*	31%	Λ	21%
η	16%	ϕ	38%	Ξ	26%

INCLUSIVE CROSS SECTION RESULTS

General Technical Comments

All data discussed in the following has been obtained with modern 4π detectors at electron-positron storage rings. Detectors usually feature a main tracking chamber operated in a solenoidal field, able to track charged particles emitted at angles larger than 20 to 30° from the beam line with efficiencies exceeding 95% for particles with momenta above 50 to 150 MeV/c. All detectors feature electromagnetic calorimetry for photon detection. Optional elements include vertex chambers and particle identification. The selection of annihilation events always requires a minimum number of charged particles (3-5) and a minimum energy seen in the detector (25-40% of $\sqrt{s}$). Additional cuts on event topology reject tau pairs and two-photon reactions. In particular at the higher energies, hadronic event samples are very clean, with typically 0.5% contamination from tau pairs, and 1% to 2% from two-photon reactions.

Cross sections such as $(1/\sigma\beta)(d\sigma/dx)$ are extracted from the raw data using corrections derived from detailed, very detector-specific Monte Carlo simulations. The following corrections have to be applied: 1) correction for acceptance losses, misidentification, backgrounds, and finite resolution, 2) correction for the bias introduced by the event selection, and 3) correction for QED radiative effects. The first set of these corrections is, at least in principle, well-defined and always applied. The second correction is occasionally neglected: due to the minimum-multiplicity requirement, the selection algorithms for hadronic events tend to bias against events with very high-momentum tracks; however, over most of the kinematic range this corrections is small. Finally, significant effects are caused by QED initial state radiation. The emission of a photon before the annihilation reduces the effective cms energy (on average by almost two GeV at PEP or PETRA energies), resulting in an increased total cross section, in a reduction of hadron cross sections near the kinematic limit

$E \approx \sqrt{s}/2$ and in a reduction of the mean number of hadrons produced per event. Since the size of these effects depends on the detector-specific event selection, cross sections have to be corrected back to the values for interactions at the nominal $\sqrt{s}$. Unfortunately, it is often unclear if radiative corrections have been applied to the published inclusive spectra, only to the quoted total cross section, or not at all.

Data Overview

We concentrate on hadron production in e^+e^- annihilation at energies around 10 GeV and above. Published data cover the Υ region around $\sqrt{s}$ = 10 GeV, the PEP energy of $\sqrt{s}$ = 29 GeV, and the typical PETRA energy around $\sqrt{s}$ = 35 GeV, with some low-statistics data points from PETRA running at intermediate energies of $\sqrt{s}$ = 12, 14, and 22 GeV. We exclude the region well below the Upsilon since most data was taken near the various charmed hadron thresholds. Inclusive spectra and total multiplicities always represent averages over all quark species; data on particle composition in quark-flavor tagged jets are scarce and suffer from large statistical errors. After a general overview, detailed discussions follow in the appropriate sections of this review.

Average hadron multiplicities per event at $\sqrt{s}$ = 10 and at $\sqrt{s}$=29 GeV, averaged over experiments (32-90), are summarized in Table 2. *Here as elsewhere in this review, numbers include antiparticles, and decay products of hyperons and* K^o_S. In the averaging of PEP and PETRA data, PETRA data are scaled (by ≈ 6-10%) to $\sqrt{s}$ = 29 GeV assuming the energy dependence predicted by the Lund model. The error associated with the model dependence of the correction is negligible compared to other experimental uncertainties. Errors are calculated based on the procedures used by the Particle Data Group (91), assuming that experiments are uncorrelated (except for uncertainties entering via branching fractions). Statistical and systematic errors are combined in quadrature.

Table 2: Average hadron multiplicities

	Particle	$\sqrt{s} \approx 10$ GeV	Ref.	$\sqrt{s} = 29$ GeV	Ref.
Pseudoscalar mesons	π^+	8.3 ± 0.4	(33)	10.3 ± 0.4	(34-36)
	π^o	3.4 ± 0.5	(33,32)	5.6 ± 0.3	(37-41)
	K^+	1.3 ± 0.2	(33)	1.48 ± 0.09	(34-36,42)
	K^o	0.92 ± 0.12	(33)	1.42 ± 0.07	(42-47)
	η	0.42 ± 0.16	(20,32)	0.60 ± 0.08	(38,48,49)
	η'	—		0.26 ± 0.10	(49)
	D^+	0.15 ± 0.04	(50,51)	0.13 ± 0.03	(52)
	D^o	0.42 ± 0.07	(50,51)	0.39 ± 0.07	(52)
	D_s		(50,32,53)		(55,56)
Vector mesons	ρ^o	0.50 ± 0.09	(33)	0.81 ± 0.08	(57-60)
	K^{*+}	0.45 ± 0.08	(33)	0.64 ± 0.05	(57,59,62)
	K^{*o}	0.38 ± 0.09	(33)	0.56 ± 0.06	(47,58,59)
	ϕ	0.045 ± 0.007	(31,33)	0.085 ± 0.011	(55,61)
	D^{*+}	0.24 ± 0.04	(50,63)	0.24 ± 0.04	(52,64-69)
	D^{*o}	0.23 ± 0.06	(50)	0.41 ± 0.11	(70,71)
	D_s^*		(72)		(70,73)
Tensor mesons	$f_2(1270)$		(33)	0.14 ± 0.04	(74)
	$K_2^{*+}(1430)$	—		0.09 ± 0.03	(62)
	$K_2^{*o}(1430)$	—		0.12 ± 0.06	(74)
?	$f_o(975)$	—		0.06 ± 0.03	(74)
?	$D^{*o}(2420)$	0.031 ± 0.010	(75,76)	—	
Octet baryons	p	0.28 ± 0.07	(33,77)	0.58 ± 0.05	(34-36)
	Λ	0.080 ± 0.013	(33,77)	0.214 ± 0.012	(46,78-81)
	Σ^o	0.023 ± 0.008	(77)	—	
	Ξ^-	0.0059± 0.0008	(33,77)	0.0178± 0.0036	(82-85)
Decuplet baryons	Δ^{++}	—		< 0.10 (95%)	(87)
	$\Sigma^{*\pm}$	0.0107± 0.0020	(77)	0.035 ± 0.009	(78,82,87)
	Ξ^{*o}	0.0015± 0.0006	(77)	< 0.006 (90%)	(83)
	Ω^-	0.0007± 0.0004	(77)	0.015 ± 0.007	(78,88)
Other bar.	$\Lambda(1520)$	0.010 ± 0.002	(86)	—	
	Λ_c	0.19 ± 0.08	(32,89)	—	
	$\bar{d}$	$(1.6\ ^{+1.0}_{-0.7})\ 10^{-5}$	(90)		

These results are graphically presented in Figure 3, where the mean number of hadrons per event per charge state and spin state is shown as a function of hadron mass. Within factors 2-3, hadron rates $\bar{n}$ exhibit an exponential mass dependence over almost 4 orders of magnitude in mass: $\bar{n} \sim \exp(-m/m_0)$, with $m_0 \approx 0.2$ GeV. Separate fits to the data on non-strange mesons and on strange mesons result in consistent slopes for the two classes, but indicate a suppression of strange hadrons by nearly a factor two, at any given mass. Multi-ply-strange hadrons are suppressed further. Also shown in Figure 3 are model predictions based on local hadron-parton duality (11). The dotted line data indicates the number of partons at a virtuality scale $Q_0 = m$. The full line shows the number of partons divided by the density of hadron states, and is the more relevant curve for comparison with experimental rates for a given hadron state. The density of states is calculated from the known meson and baryon states and is smoothed by convoluting it with a gaussian of width 0.1 GeV. Given the minimal assumptions and the neglect of effects due to quantum number conservation, the agreement with data is quite remarkable.

In Figure 4 the experimental average multiplicities are compared with results from Monte-Carlo hadronization models, namely the Lund Model (Version 6.3) (92), the Webber model (Version 4.1) (13) and the Caltech model (Version II) (21). We use these three models in all following comparisons, since they represent extremes in the string approach (Lund) and in the QCD cluster approach (Webber), and an intermediate point of view emphasizing the use of low-energy data to reduce the number of input assumptions (Caltech). In all cases, the default model parameters are used. The agreement between data and models for different classes of hadrons is summarized in Table 3. We note that in this global comparison, the Lund model is closest to the data.

The variation of mean multiplicities between $\sqrt{s} \approx 10$ GeV and $\sqrt{s} \approx 30$ GeV is illustrated in Figure 5. Most notable is the larger rise of multiplicity with $\sqrt{s}$ for baryons as compared

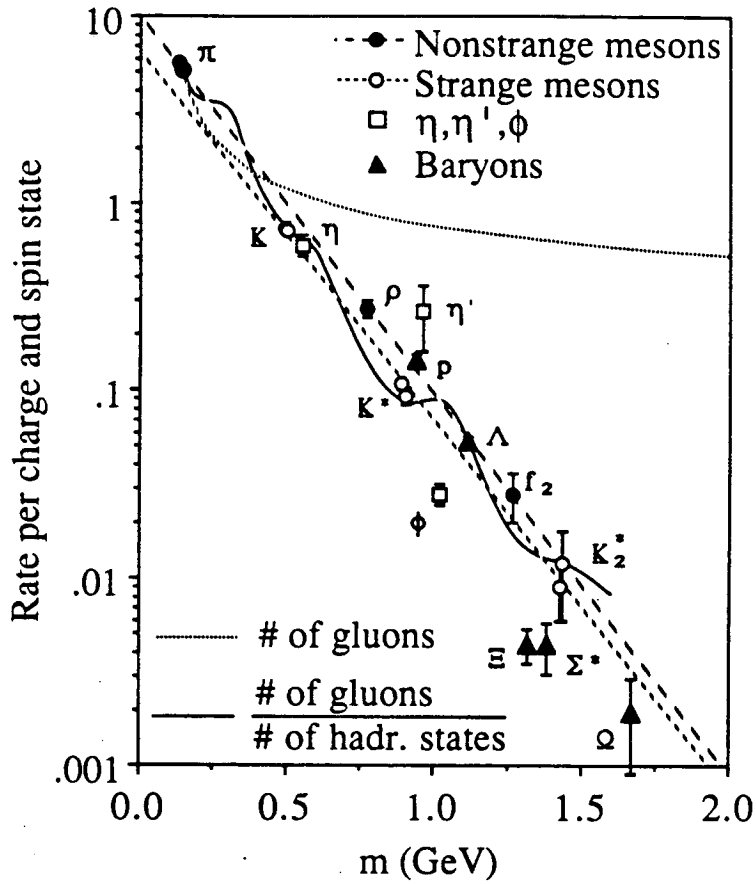

Figure 3 Mean number of hadrons produced per charge and spin state, as a function of hadron mass m, for e^+e^- annihilation events at $\sqrt{s}$ = 29 GeV. Data are averaged over PEP and PETRA experiments (see Table 2). Long-dashed and short-dashed lines: exponential fits of the form $N\exp(-m/m_0)$. Fits to the nonstrange-meson rates (π,ρ,f_2) and to strange-meson rates (K,K^*,K_2^*) yield N=10.1, m_0=0.215 GeV and N=6.4, m_0=0.222 GeV, respectively. Dotted line: mean number of gluons of virtuality Q_0 = m in the parton shower, using $\Lambda_{QCD} = m_\pi$. Full line: mean number of gluons in parton cascade, divided by the (smoothed) density of hadronic states. Both the dotted and the full curve are rescaled (by factors of order 2) to match the π data point.

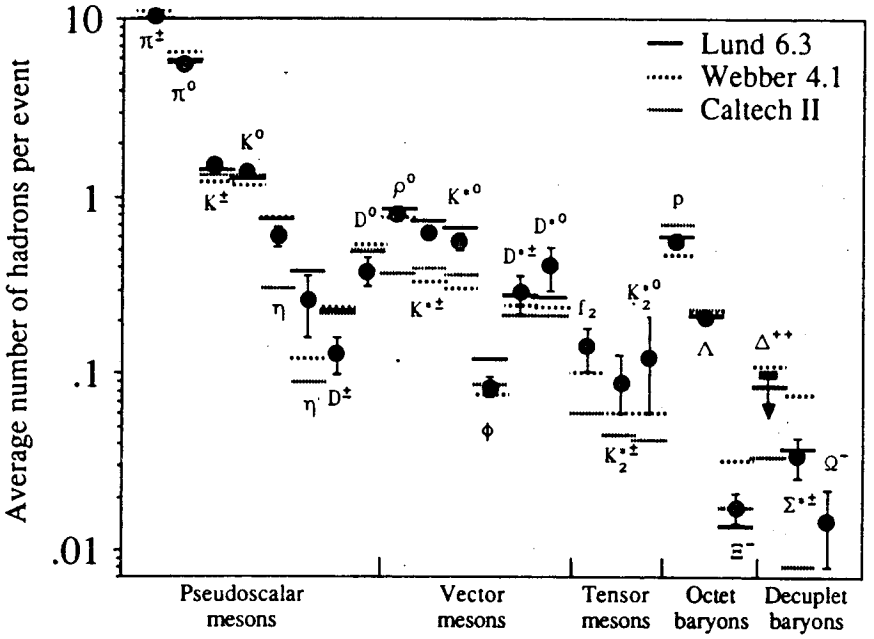

Figure 4 Average number of hadrons per event produced in e^+e^- annihilation at $\sqrt{s}$ = 29 GeV, compared to results of the Lund Vs. 6.3 (———), Webber Vs. 4 (·····), and Caltech II (·····) Monte Carlo models. Data are averaged over PEP and PETRA experiments (see Table 2). All models use the default parameters supplied by their authors.

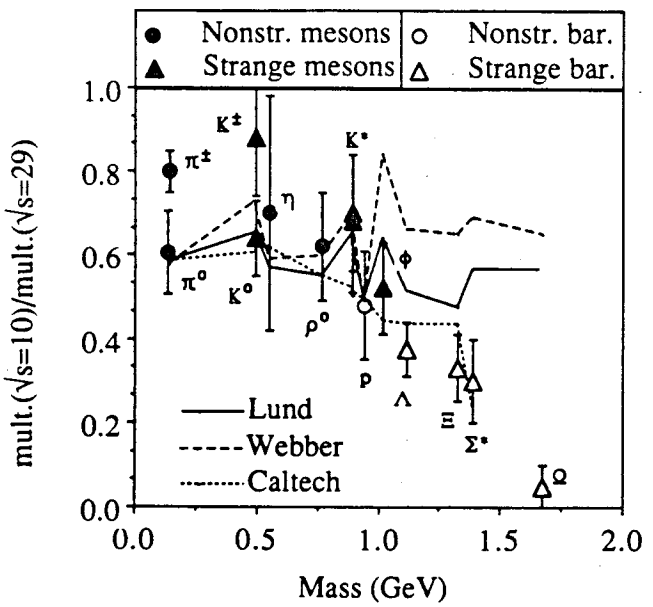

Figure 5 Ratio of average hadron multiplicities per event at $\sqrt{s} \approx 10$ GeV and at $\sqrt{s} = 29$ GeV as a function of hadron mass, together with predictions of the Monte Carlo fragmentation models Lund Vs. 6.3 (———), Webber Vs. 4.1 (- - - - -), and Caltech II (·····). All models use the default parameters supplied by their authors. Data from Table 2.

Table 3: Agreement between measured and predicted multiplicities, expressed in terms of a $\chi 2$.

Model:		Lund (6.3)		Webber (4.1)		Caltech (II)	
$\sqrt{s}$ (GeV):		10	29	10	29	10	29
Sample	NDF						
Pseudoscalar mesons	7,8	40.0	23.7	27.8	54.7	52.5	31.1
Vector mesons	6	23.8	20.8	17.2	52.9	17.5	69.0
Tensor mesons	–,3	no prediction		—	3.0	—	8.1
Octet baryons	4,3	7.7	1.6	239.3	18.1	8.2	9.8
Decuplet baryons	3,4	12.3	6.6	353.4	42.3	19.0	13.9
Total, excl. tensors	20	83.8	52.7	638	171.0	97.2	131.9

NDF stands for the number of input data points (at 10 and 29 GeV). Model predictions are based on the default parameter settings. Improvements are possible using modified parameters, but at least within the (limited) range explored by the author the relative ranking of the models remains essentially the same.

to mesons, which is not reproduced by the Lund and Webber models. The $\sqrt{s}$ dependence of Ω^- rates appears particularly drastic; however, due to the large error in the denominator the data point is consistent with unity within 2 S.D.

INCLUSIVE PRODUCTION OF CHARGED STABLE HADRONS

The largest body of data on particle composition in jets concerns the inclusive production of charged stable hadrons $\pi^{\pm}$, $K^{\pm}$ and $p,\bar{p}$, and their production ratios. From the average multiplicities per event, a strong SU(3) breaking is evident. It is striking to find a baryon rate as high as 1/3 of the kaon yield.

Momentum Distributions and Particle Composition

A compilation of PEP and PETRA data on scaled $\pi^{\pm}$, $K^{\pm}$ and $p,\bar{p}$ cross sections as a function of $x=2E/\sqrt{s}$ is shown in Figure 6. Different experiments agree reasonably well, with the exception of the low-momentum data on kaon production, where in particular the TASSO data and the TPC data diverge slightly. Within the experimental precision, TASSO cross sections $(s/\beta)(d\sigma/dx)$ do scale according to Equations (2,3) over the PETRA energy range (Figure 7). Therefore, the problems in the low-x kaon data cannot be explained in terms of threshold effects.

In the large-x region, cross sections are well-described by a $\frac{(1-x)^n}{x}$ dependence. Fits to the TPC data above $x = 0.5$ yield $n = 2.24\pm0.16$, 2.79 ± 0.29 and 1.61 ± 0.53 for $\pi^{\pm}$, $K^{\pm}$ and $p,\bar{p}$, respectively. A fit to the sum of the three cross sections yields $n = 2.36\pm0.14$.

Results on particle composition are usually expressed in terms of particle fractions or ratios, typically as a function of the scaled momentum $z = p/p_{beam}$ as the directly measured variable. A compilation of PEP and PETRA results on charged-hadron fractions is shown in Figure 8(a); the crowded low-momentum region is expanded in Figure 8(b). The kaon

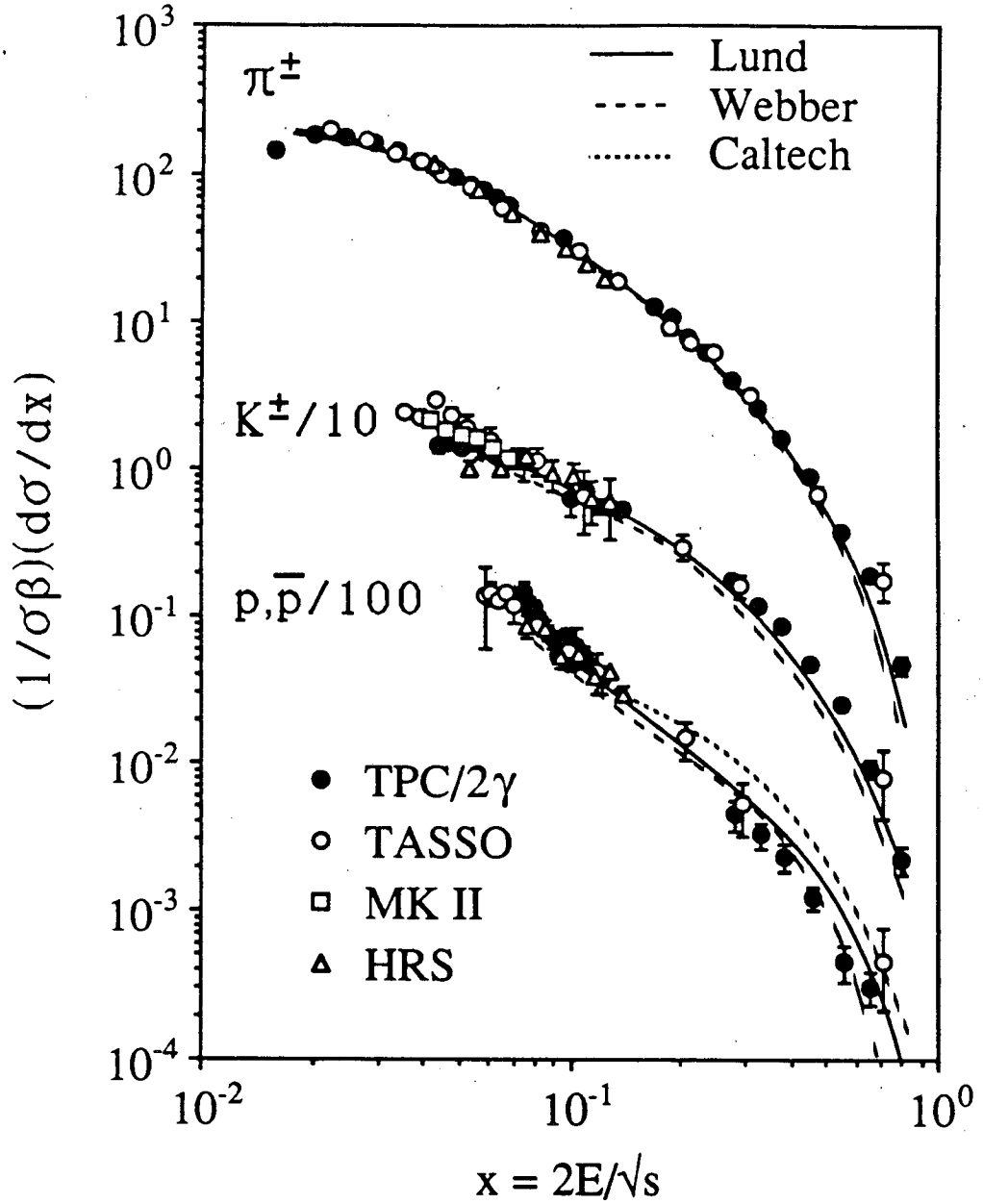

Figure 6 Inclusive scaled cross sections $(1/\sigma\beta)(d\sigma/dx)$ for production of charged pions, kaons and protons in e^+e^- annihilation at $\sqrt{s} \approx 30$ GeV, as a function of $x = 2E/\sqrt{s}$. Data: HRS (34), MARK II (42),TASSO (35), and TPC/2γ (36). Lines indicate predictions of fragmentation models (see Figure 5).

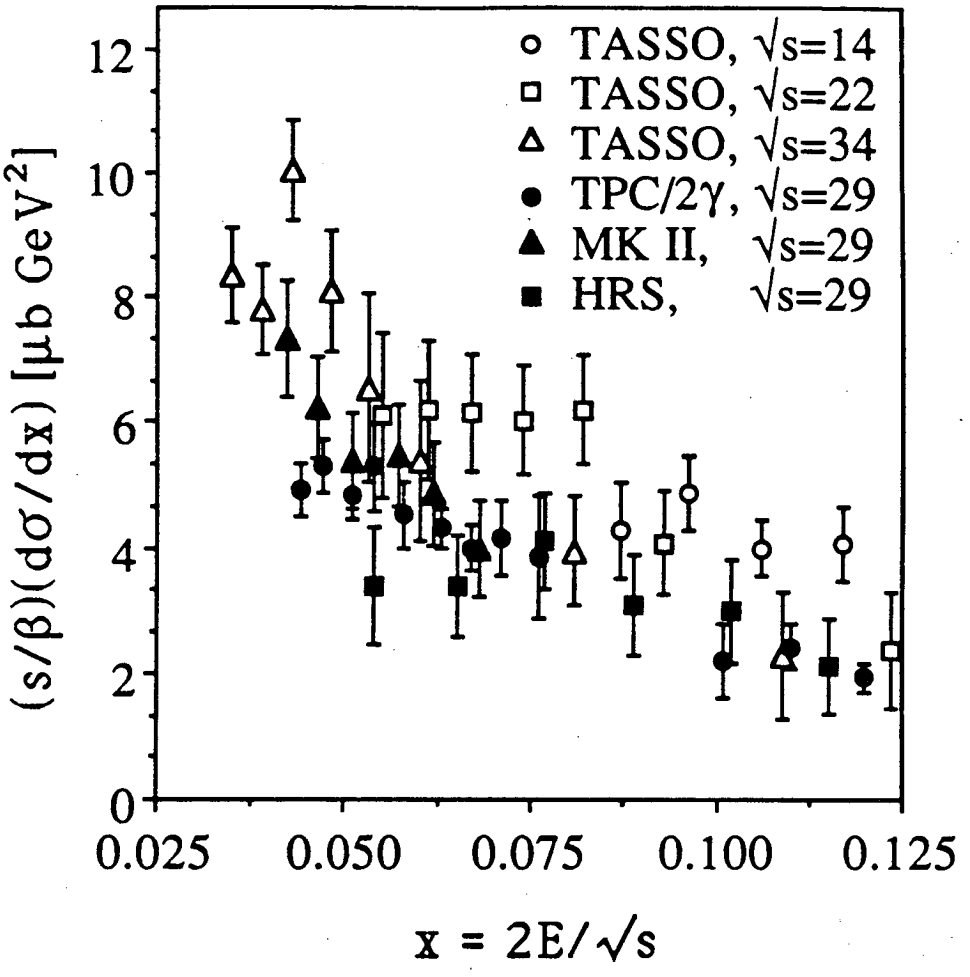

Figure 7 Scaling behaviour of the cross section $(s/\beta)(d\sigma/dx)$ for charged-kaon production, for $\sqrt{s}$ = 14, 22, 29, and 34 GeV. Data from TASSO (35), HRS (34), MARK II (42) and TPC/2γ (36).

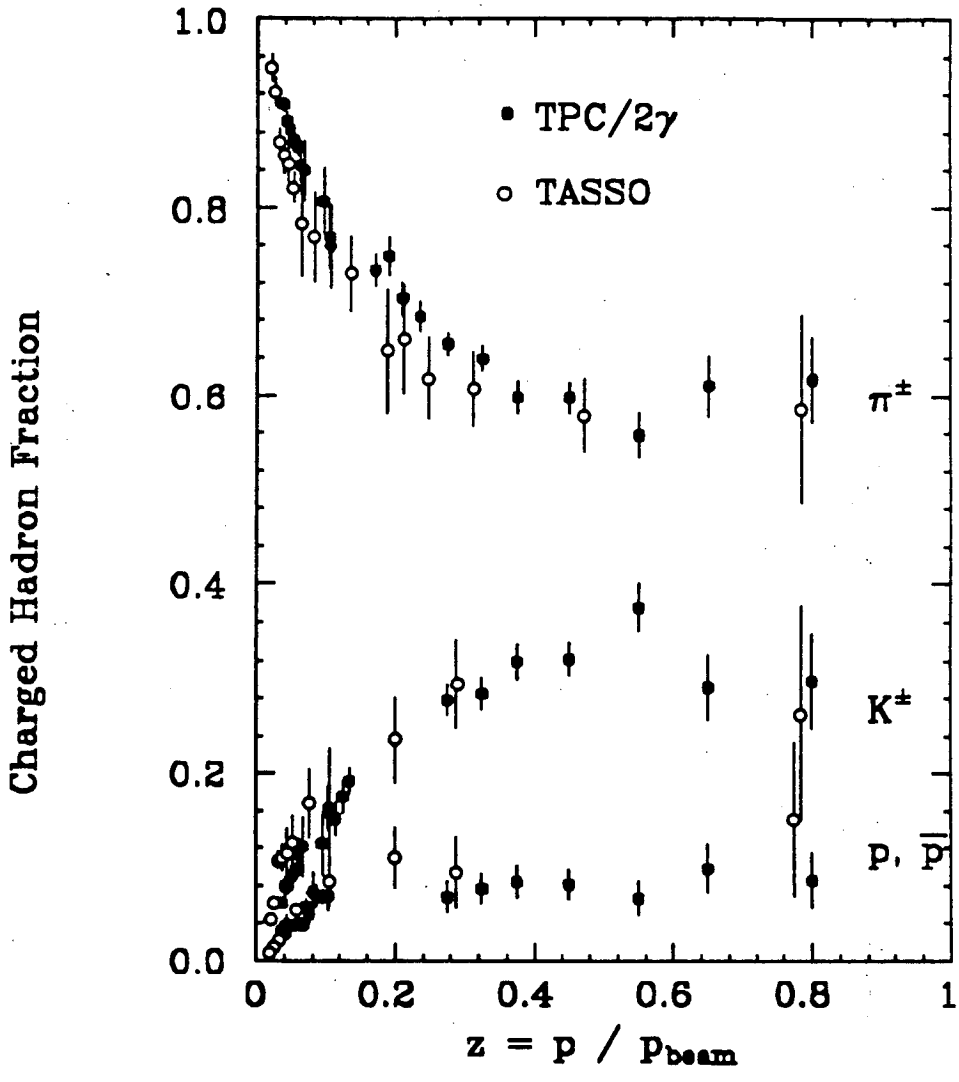

Figure 8(a) Fraction of pions, kaons, and protons among charged hadrons produced in e^+e^- annihilation at $\sqrt{s} \approx 30$ GeV, as a function of the scaled momentum $z = p/p_{beam}$. Data: TASSO (35) and TPC/2γ (36).

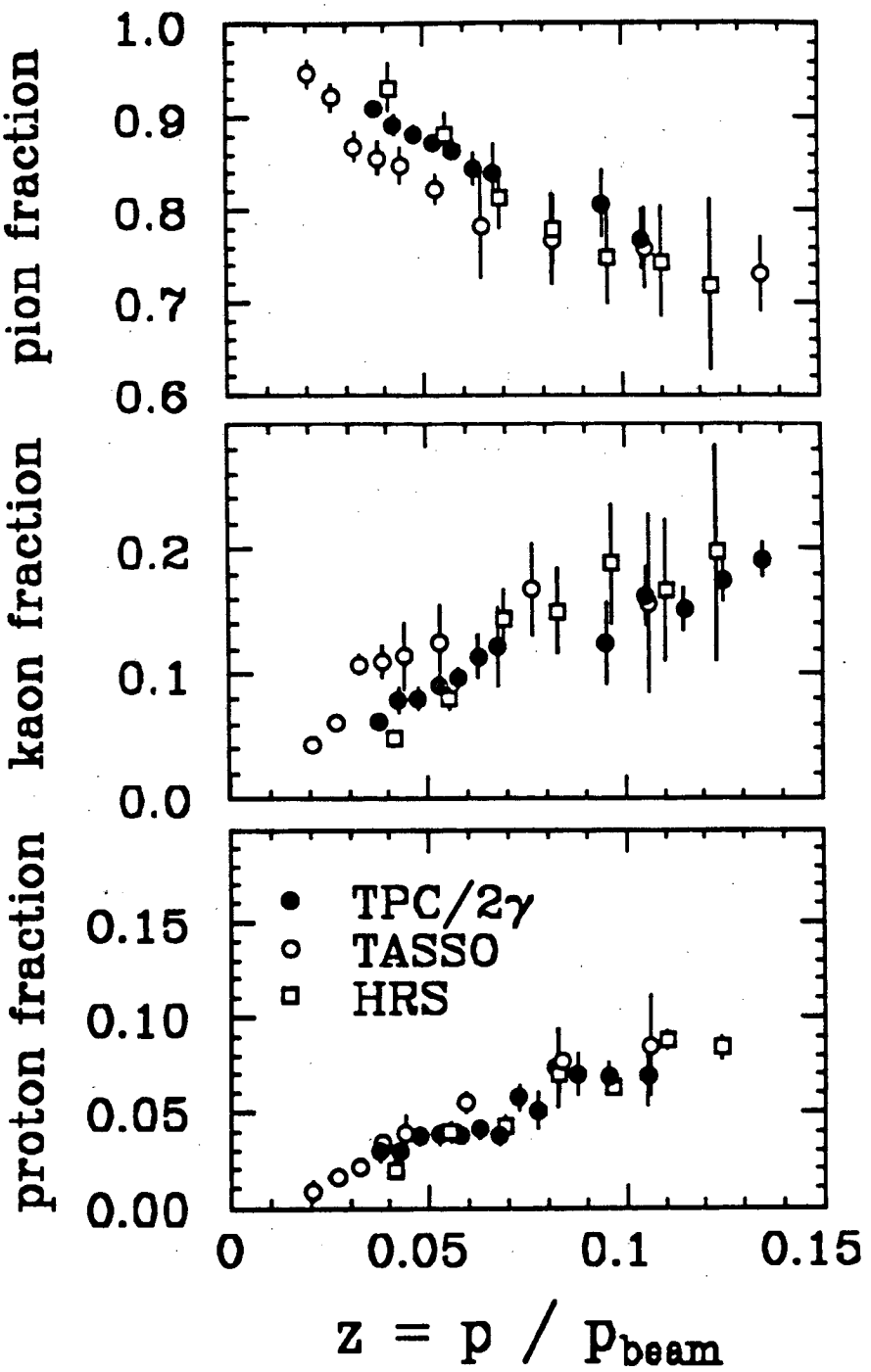

Figure 8(b) Expanded view of the low-z region, also showing HRS data (34).

and proton fractions rise with z, leveling off at $z \approx 0.3$ at values around 30% and 8%, respectively.

Understanding Inclusive Distributions and Particle Fractions

Much of the momentum dependence of cross sections and fractions can be understood in term of several rather benign effects which, collectively, go a long way towards explaining the observations.

Fragmentation dynamics is perceived to work essentially in one dimension. In effect, the phase space between initial q and $\bar{q}$ is more or less uniformly sprinkled with new $q\bar{q}$ pairs, followed by local recombination into hadrons. It is therefore not surprising that the gross features of hadron distributions reflect one-dimensional multiparticle phase space. Longitudinal phase space yields the scaling limit of the fragmentation functions D(x) (93):

$$\frac{1}{\sigma_{tot}} \times \frac{d\sigma_h}{dx} = 2 \times D(x) \approx 2\,(n+1)\,(1-x)^n \qquad (6)$$

(under the simplifying assumption that only one hadron species is produced). At low momenta (small compared to typical transverse momenta of particles in jets), one expects a constant Lorentz invariant cross section $E\frac{d^3\sigma}{d^3p}$, resulting in

$$\frac{d\sigma}{dz} \sim \frac{d\sigma}{dp} \sim \beta p \qquad (7).$$

Equation (7) accounts for the rise in heavy-particle fractions at low momentum, until all species are relativistic.

The production rates of unstable hadrons (to be discussed later) hint that few of the observed stable hadrons are produced directly in the confinement process. Instead, they are mostly decay products of short-lived resonances. This is illustrated in Figure 9, based on a simulation using the Lund fragmentation model. The main effect of decays is a modest softening of proton and kaon spectra (compared to the primary baryons and strange

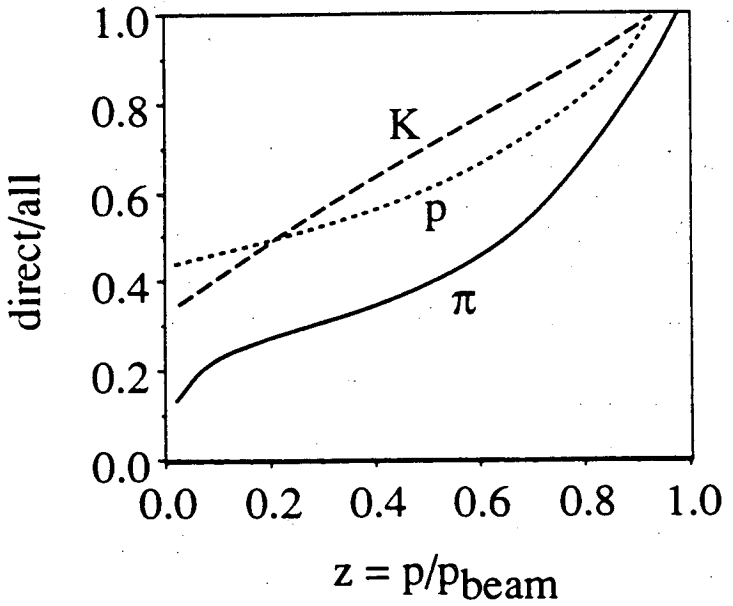

Figure 9 Fraction of directly produced charged hadrons (as opposed to decay products of resonances), in $u\bar{u}$-events as a function of z, using the Lund Monte Carlo generator.

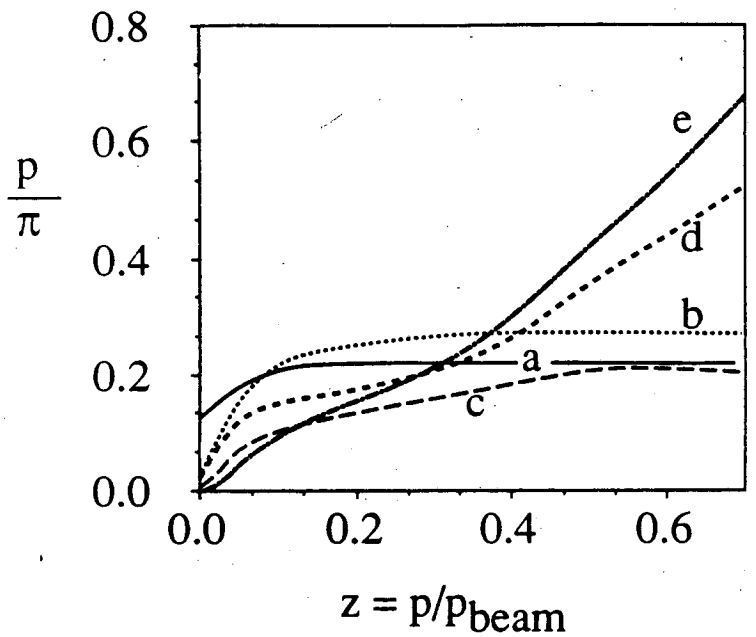

Figure 10 Ratio of charged protons to pions in $u\bar{u}$-events as a function of z, as generated by the Lund Monte Carlo generator. Curve 'a': 2-jet events using a flavor-independent fragmentation function of the Feynman-Field type, before resonance decays; 'b': same, but including multi-jet events with boosted strings; 'c': as 'a', but after resonance decays. Curve 'd': 2-jet events using the mass-dependent symmetric fragmentation function, before resonance decays; 'e': same, but including multi-jet events with boosted strings, after resonance decays.

hadrons, respectively) and a large increase in the rate of soft pions. For an identical x dependence of primary production of nonstrange and strange mesons and of baryons, the observed K and p fractions among final stable hadrons therefore continue to rise through the intermediate x range, and level off at large x , where direct production dominates.

Another fairly general feature of particle production is that particle sources, be it color strings or clusters, move with respect to the cms. Since typical momenta in the rest frame of the source are of the same scale as particle masses, boost effects result in the increase of heavy-particle fractions with cms momentum. The effects of phase space, decays and boost effects on the p/π ratio are exemplified in Figure 10, based on the Lund model.

Comparison with Models

All models reproduce the inclusive pion spectra fairly well (Figure 6). The reason is simple: model parameters are adjusted to reproduce the average multiplicity of charged hadrons, mostly pions. Correct mean hadron multiplicity however almost automatically implies correct inclusive spectra, except for the high-x region. Early QCD cluster models indeed underpredicted the data at very large $x \approx 1$, but this problem has since been fixed by identifying low-mass clusters directly with hadrons.

However, all models have significant difficulties describing the z-dependence of particle ratios. Since a disagreement in the cross section of one species propagates into the fractions of all three species, we present the comparison in terms of kaon/pion and proton/pion ratios, indicative of the relative suppression of strange-hadron and of baryon production (Figure 11). At low z, kinematic effects dominate and models tend to agree among themselves and with the data (normalization problems at the 10-20% level in the particle ratios can usually be fixed by changes in the model parameters). With increasing z, however, serious discrepancies in the z-dependence of the p/π^+ ratio become apparent for all models.

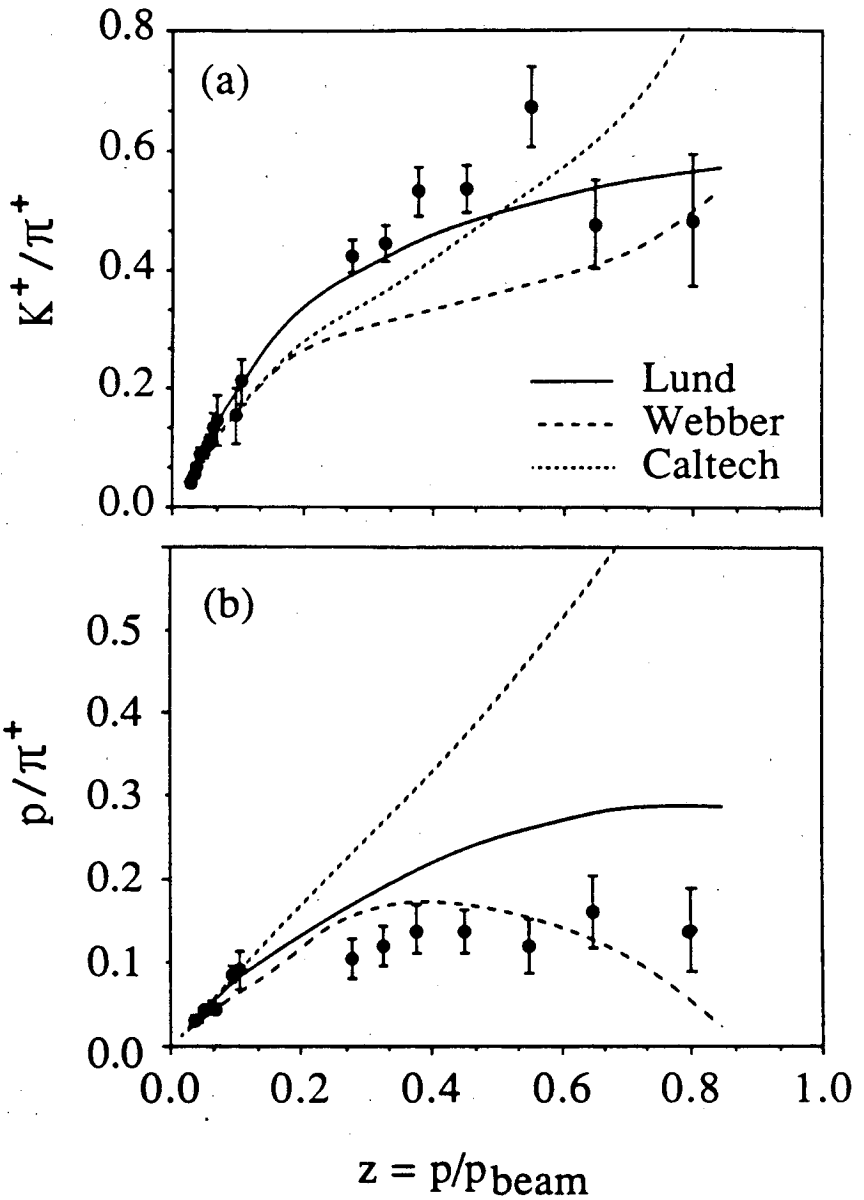

Figure 11 (a) Ratio of production rates of charged kaons and pions in e^+e^- annihilation at $\sqrt{s}$ = 29 GeV, as a function of the scaled momentum $z = p/p_{beam}$. Data: TPC/2γ (36). Lines indicate predictions of fragmentation models (see Figure 5). (b) Ratio of proton and pion production rates.

In case of the Lund model, a possible fix is to introduce a flavor-dependence of the 'a' parameter in f(z) (Equation (5)). In the case of the two QCD cluster models, modifications in the treatment of the leading clusters (which are atypical in that they contain one of the initial quarks) are required.

Two semi-quantitative pictures should be mentioned here: dimensional counting rules (DCR) (1,2) and calculations based on local parton-hadron duality (11). Counting rules predict that exponents n in the $(1-x)^n$ dependence of high-x cross sections differ by (at least) one unit for π's and p's: $n_p - n_\pi \geq 1$, in disagreement with experimental result $n_p - n_\pi = -0.63 \pm 0.55$ for $x > 0.5$. A possible excuse is that DCR's are supposed to hold only for $x \rightarrow 1$, and that nobody really knows at which x DCR behavior sets in (at $x \approx 0.5$, $x \approx 0.9$, $x \approx 0.99$?).

Local hadron-parton duality predicts that the spectra of hadrons of mass m correspond to the spectra of partons in a parton shower with cutoff $Q_0 = m$. With the advent of more precise data, the good agreement model and reality reported earlier (11) suffers somewhat (Figure 12); however given the minimal input and the fact that even the normalization of spectra is predicted within 30% (Figure 2), the result is still very satisfactorily. Futhermore, deviations are expected at high z and at very low z. Firstly, the calculations refer to the spectrum of gluons in a gluon jet; the spectra of partons in quark jets differ in particular near $x \approx 1$. Secondly, there is some ambiguity in the interpretation of the scaling variable (energy, momentum, ...) for non-relativistic hadrons, which influences predictions up to $z \approx 2M/p_{beam} \approx 0.02$ (π), 0.07 (K), 0.13 (p).

Rapidity and Transverse-Momentum Distributions

While most data on hadron production is published in the form of momentum dependent cross sections, this is by no means the only, or even the most natural way to present the

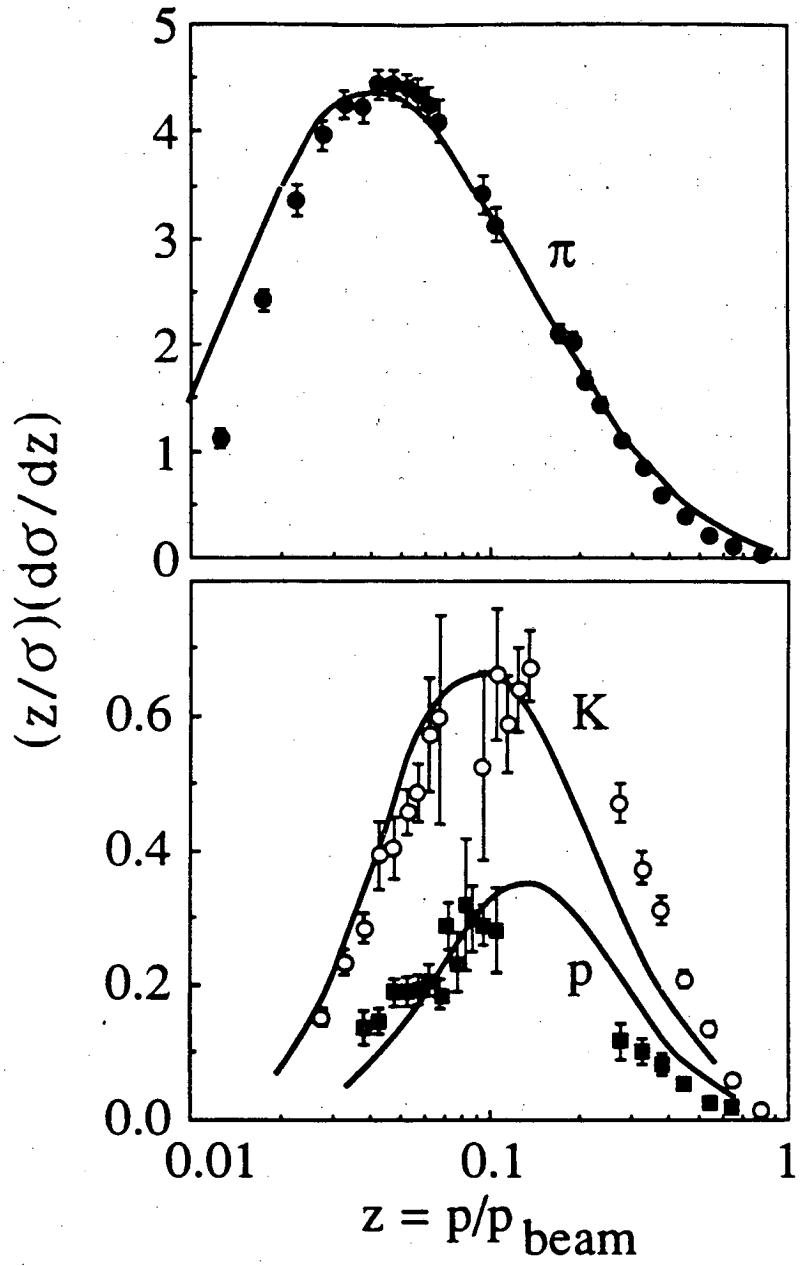

Figure 12 (a) Inclusive production rates $(z/\sigma)(d\sigma/dz)$ of charged pions, kaons and protons in e^+e^- annihilation at $\sqrt{s}$ = 29 GeV, as a function of the scaled momentum $z = p/p_{beam}$, compared to (arbitrarily normalized) predictions based on hadron-parton duality (11). Data: TPC/2γ (36).

data. In trying to understand hadronization phenomena, it is very helpful to study hadron composition as a function of the rapidity $y = \frac{1}{2} \log\left(\frac{E+p_{\parallel}}{E-p_{\parallel}}\right)$, defined with respect to the sphericity or thrust axis. Longitudinal phase space corresponds to a flat rapidity distribution $d\sigma/dy$ in the central region around $y \approx 0$, falling off smoothly in the fragmentation regions at high rapidity. Since the initial quarks have a high rapidity $y \approx \pm\log(\sqrt{s}/m_q)$, and since the confinement process involves only limited momentum transfers and correspondingly small shifts in rapidity, the fragmentation regions are populated by particles containing the primary quark or the antiquark. The central region contains mainly particles made of newly formed quarks. At PEP and PETRA energies the kinematic range in y (± 5 units for pions) is large enough for a reasonably clean separation of central region and fragmentation regions.

Figure 13 shows the cross sections of $\pi^{\pm}$, $K^{\pm}$ and $p,\bar{p}$ as a function of $|y|$, as well as the corresponding particle ratios. In the central region, cross section and fractions are approximately constant. The fraction of kaons increases at higher rapidity due to strange-particle production in the decays of charmed hadrons concentrated around $|y| \approx 2$. Kinematical effects cause kaon and proton fractions to drop at $|y| > 3$. Fragmentation models are in fair agreement with data; the problems in the high-y proton fractions reflect the behavior at large x.

Both at fixed y and integrated over all y, the particle composition varies with the transverse momentum p_T with respect to the jet axis. Figure 14 displays π, K and p fractions as a function of p_T with respect to the thrust axis. Heavy hadrons show a significantly flatter p_T distribution than pions. As with momentum distributions, the rise of heavy-hadron fractions at low p_T is caused by kinematical effects and by an enhancement of low-p_T pion rates due to resonance decays. This is evidenced in particular by the Lund model predictions; there, all primary hadrons are generated with the same average p_T with respect to the

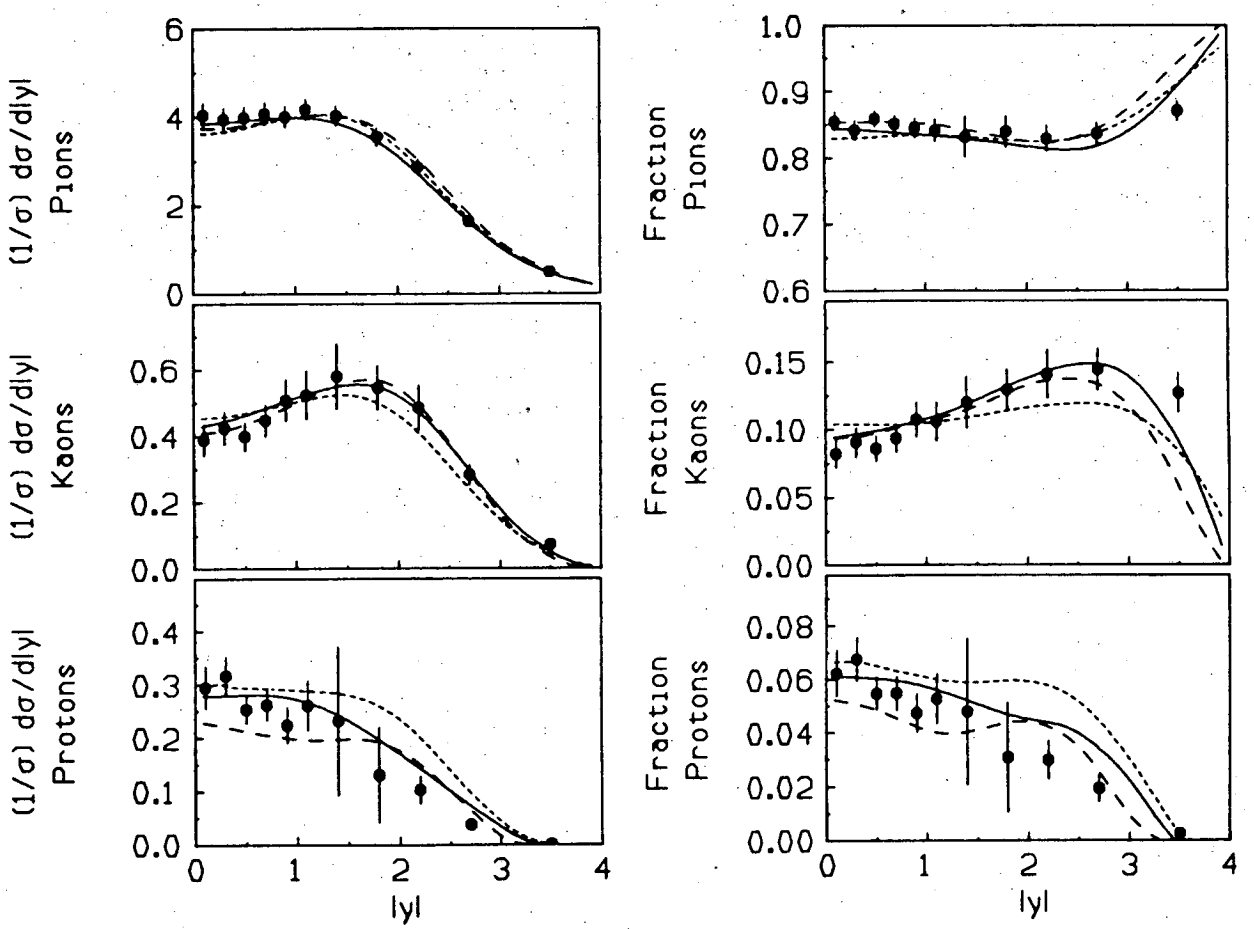

Figure 13 (a) Inclusive cross sections $(1/\sigma)(d\sigma/d|y|)$ for production of charged pions, kaons, and protons in e^+e^- annihilation at $\sqrt{s}$ = 29 GeV, as a function of the rapidity y defined with respect to the sphericity axis. Data: TPC/2γ (36). Lines indicate predictions of fragmentation models (see Figure 5). (b) Charged-hadron fractions as a function of rapidity.

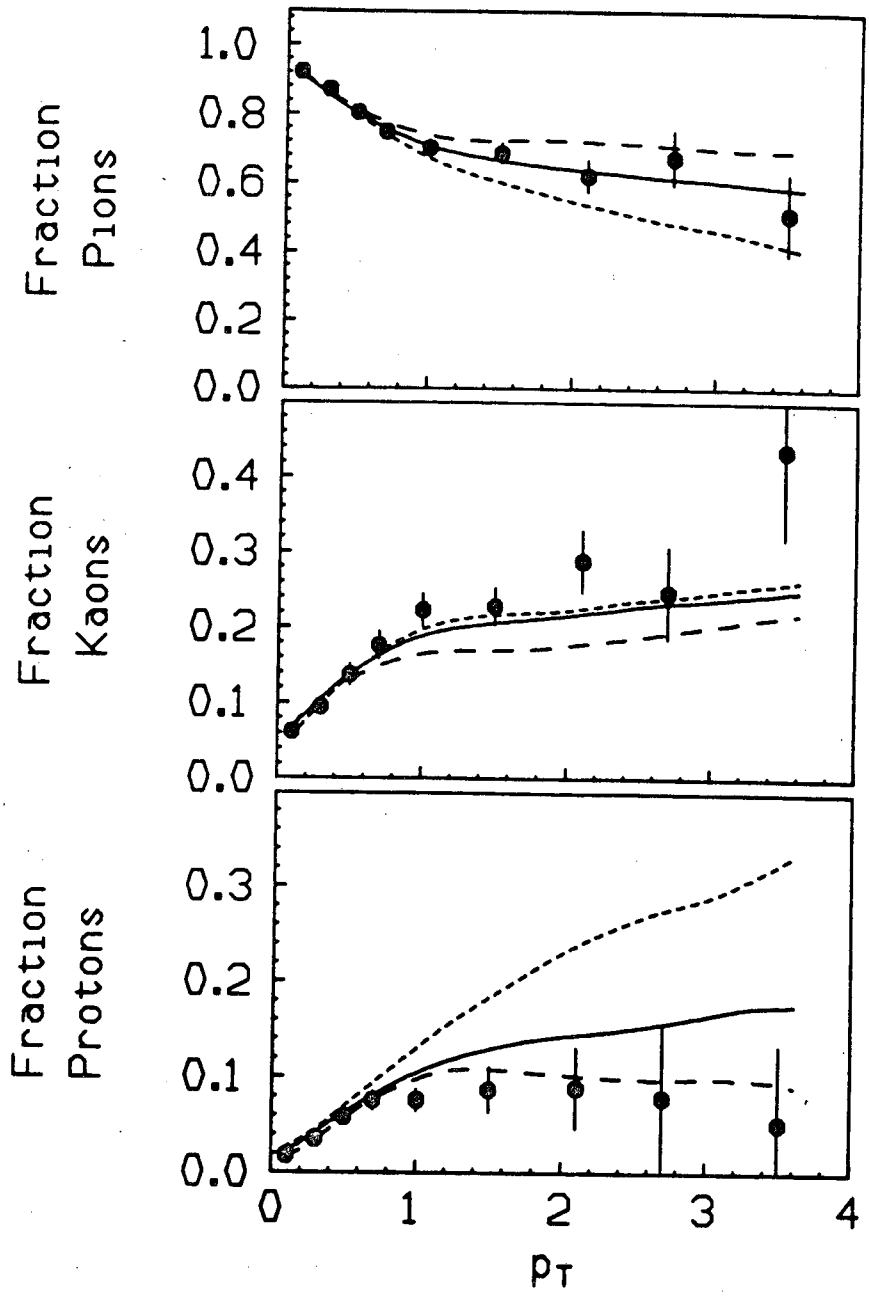

Figure 14 Fraction of pions, kaons, and protons among charged hadrons produced in e^+e^- annihilation at $\sqrt{s}$ = 29 GeV, as a function of the transverse momentum p_T defined with respect to the thrust axis. Data: TPC/2γ (36). Lines indicate predictions of fragmentation models (see Figure 5).

string and any p_T dependence is created at later stages. Differences between models start to show up at higher p_T's, where the measured fractions level off. Three-jet events dominate particle production in this region, and the fractions essentially reflect the momentum dependence of the fractions shown in Figure 8.

THE SU(3) MESONS

Production rates of higher-mass mesons take a central role in the investigation of fragmentation phenomenology, since most stable hadrons are produced in resonance decays. Unfortunately, the investigation of resonance production faces numerous difficulties in the cross section measurements, either due to combinatorial backgrounds, low production rates, or both. Typical statistical and systematic errors range from 10% to over 50%. Measurements are usually presented as a function of momentum; often, the low-momentum region is missing because backgrounds swamp the signal. We will concentrate mainly on data from PEP and PETRA because of their (usually) higher precision and because of the smaller (relative) contributions from to heavy-quark decays.

Inclusive Production Cross Sections

All mesons in the SU(3) pseudoscalar and vector nonets have been observed in e^+e^- annihilation at PEP or PETRA, with the exception of the $\rho^{\pm}$ and the ω (see Table 2). The statistical significance of resonance signals ranges from very good to quite marginal; lack of space prevents a detailed discussion. No significant spin alignment was observed for any of the vector mesons; acceptance estimates hence generally assume isotropic decay.

Figures 15(a) through 15(d) display display production cross sections $(1/\sigma\beta)(d\sigma/dx)$ for several families of mesons: (a) nonstrange mesons (π,ρ,f_2), (b) strange mesons $(K,K^*(892),K_2^*(1430))$, (c) pseudoscalar mesons (π,K,η,η') and (d) vector mesons $(\rho,K^*(892),\phi)$. The purpose of Figure 15 is threefold: firstly, to show the progression of

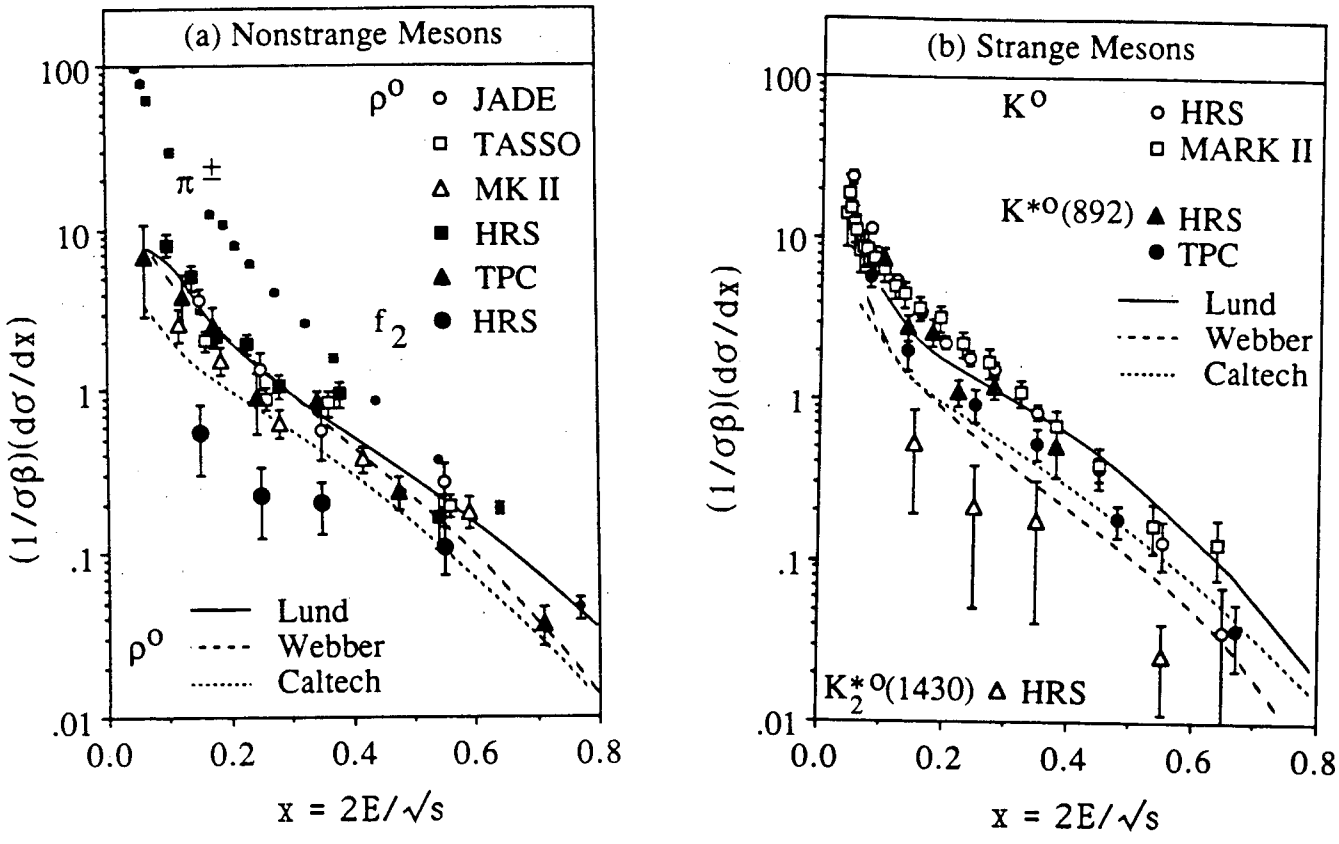

Figure 15 Inclusive cross sections $(1/\sigma\beta)(d\sigma/dx)$ for production of meson resonances in e^+e^- annihilation at $\sqrt{s} \approx 30$ GeV, as a function of $x = 2E/\sqrt{s}$. Lines indicate predictions of fragmentation models (see Figure 5).

(a) Nonstrange mesons: $\pi^{\pm}$, ρ^o, and $f_2(1270)$ (HRS (58,74), JADE (57), MARK II (59), TASSO (60), TPC/2γ (36)). Model predictions for ρ^o.

(b) Strange mesons: K^o, $K^{*o}(892)$, and $K_2^{*o}(1430)$ (HRS (58,74), MARK II (59), TPC (47)). Model predictions for K^{*o}.

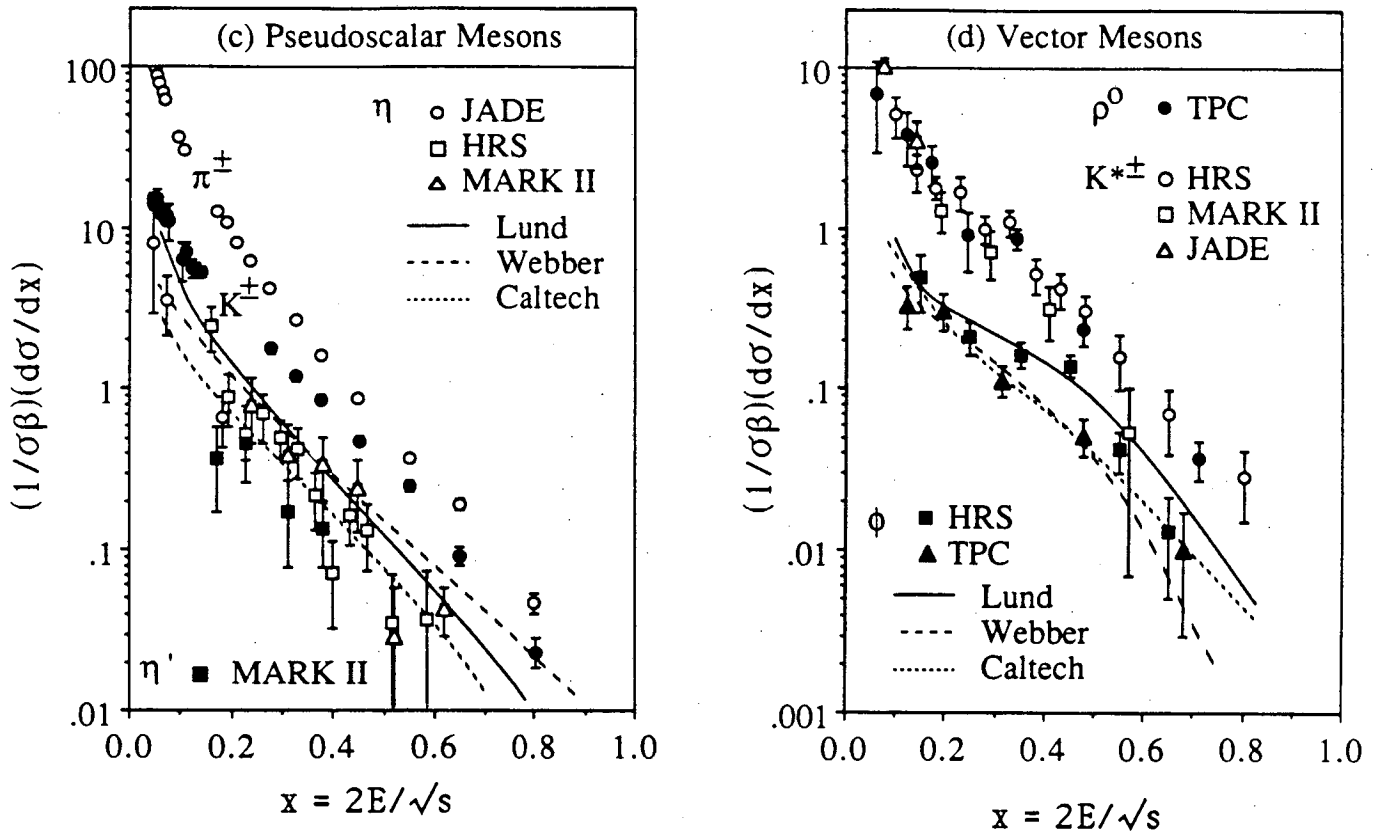

Figure 15 cont'd (c) Pseudoscalar mesons: $\pi^{\pm}$, $K^{\pm}$, η and η' (TPC/2γ (36), HRS (48), JADE (38), and MARK II (49)). Model predictions for η.
(d) Vector mesons: ρ^{o}, $K^{*\pm}(892)$, and ϕ (HRS (55,62), JADE (57), MARK II (59), TPC (61) and TPC/2γ). Model predictions for ϕ.

cross sections within a meson family, secondly, to confront results from different experiments, and finally to compare data with models. In order not to crowd the figures even more, model predictions are shown for only one species per set. Figure 15(a) shows clearly the much steeper spectrum of pions as compared to ρ-mesons, emphasizing that most pions are decay products. The agreement between experimental results on ρ cross sections is marginal; given that this cross section is difficult to measure due to the large ρ width and the enormous background, one suspects that in some cases systematics may be underestimated. Tensor mesons are suppressed by factors of order 5-10 compared to vectors; this is also evident from Figure 15(b). Figures 15(c) and (d) illustrate the suppression of strange hadron production rates within a nonet. (At first glance, the ρ - K* comparison shows equal cross sections for the two; note, however, that we show one charge state of the ρ, compared to two charge states of the K*. Also, the relative enhancement of cross sections due to charm decays is stronger for kaons - see Table 1.)

As far as the x-dependence of cross sections is concerned, data are often not precise enough to differentiate between models; the information is essentially summarized in the mean multiplicities (Tables 2,3 and Figure 4). The Lund model with default parameters yields a χ^2/NDF of about 3 for both pseudoscalar and vector mesons; most significantly, it overpredicts the ϕ rate, a problem partly related to the D_S decay branching ratios used in the Monte Carlo (31). The Webber model suffers from poor agreement in π, K and K* rates; this problem could most likely be fixed by tweaking of parameters. The Caltech II model has a tendency to underpredict vector meson rates by as much as a factor of two.

Based on the average hadron multiplicities given in Table 2, one can estimate the average number of primary hadrons before decays. We first subtract the expected yields due to charm and bottom decays from the mean multiplicity; lacking a better alternative, we use Lund-model results for this corrections and assign generous errors especially in dubious

cases such as the ϕ (see Table 1). For each species, contributions from decays of other resonances are subtracted, avoiding double counting which could arise from chain decays like $\eta' \rightarrow \eta + x$, $\eta \rightarrow \pi + x$ since both η and η' are measured. We assume $\rho^{\pm} \approx (1.9 \pm 0.1)\ \rho^{o}$ and $\omega \approx (0.95 \pm 0.05)\ \rho^{o}$. The subtractions also include effects of baryon decays. The results depend on the definition of a 'primary' hadron, which becomes vague as soon as the lifetime of a particle is similar to the confinement time scale. For example, it is clear that the "clusters" of QCD cluster models are really normal quark model states in a regime where the spacing of levels is small compared to the width of states. One clear cut is to consider only the L=0 pseudoscalar and vector nonets, and to move anything happening at earlier stages into the realm of confinement dynamics. The authors of the Lund model take this point of view. Table 4 shows the resulting rates of primary mesons at $\sqrt{s}$ = 29 GeV, for three different assumptions:

1) subtraction includes contributions from decays of pseudoscalar (P) and vector (V) mesons and of octet (O) and decuplet (D) baryons.

2) subtraction includes in addition the tensor (T) meson ($^3P_2$) nonet. The f_2' rate is not measured, but should be small compared to the $f_2(1270)$ rate. The a_2 rates are taken equal to the f_2 rate. Tensor meson production in charm and bottom decays is assumed to be negligible.

3) subtraction includes the $^1P_1$, $^3P_0$, and $^3P_1$ nonets. Since some assignments of particles to these nonets are ambiguous and since decay modes are poorly known, we assume that each nonet yields about the same rate as the $^3P_2$ nonet.

If meson multiplets beyond the pseudoscalar and vector nonets are excluded from consideration, one finds significant production of both "primary" pseudoscalars and vectors in a ratio P:V $\approx$ 3:2. Including primary tensor mesons and extrapolating to other P-wave quark states, production rates for light pseudoscalars are consistent with zero. In this case, the

Table 4: Estimated yields of primary mesons (antiparticles included)

in e^+e^- annihilation at $\sqrt{s} = 29$ GeV

multiplets considered:	P,V,O,D	P,V,T,O,D	P,V,all P waves,O,D
π^+	2.2 ± 0.7	1.6 ± 0.7	- 0.3 ± 1.1
π^o	0.87 ± 0.45	0.58 ± 0.45	-0.3 ± 0.6
K^+	0.56 ± 0.13	0.45 ± 0.13	0.12 ± 0.18
K^o	0.55 ± 0.11	0.44 ± 0.12	0.11 ± 0.16
η	0.34 ± 0.13	0.27 ± 0.14	0.06 ± 0.15
η'	0.22 ± 0.11	(*)	(*)
ρ^o	0.65 ± 0.10	0.55 ± 0.10	0.25 ± 0.16
K^{*+}	0.41 ± 0.07	0.37 ± 0.08	0.25 ± 0.11
K^{*o}	0.34 ± 0.08	0.30 ± 0.08	0.18 ± 0.11
ϕ	0.05 ± 0.03	(*)	(*)
total primary mesons (excl. C,B mesons)	8.1 ± 1.0	7.3 ± 1.0	5.1 ± 1.7
$\langle m \rangle_{prim.\ mesons}$ (excl. C,B mesons)	≈ 0.5 GeV	≈ 0.6 GeV	≈ 1.2 GeV

(*): no additional contributions known, but possible due to incompleteness of decay tables.

average mass and the number of primary mesons (Table 4) are similar to the corresponding parameters of clusters in QCD cluster models; average cluster masses in the Webber and Caltech II models are ≈ 1.5 GeV and ≈ 1.8 GeV, respectively.

Obviously, it is almost impossible to determine what the really "primary" particles are - for all we know, even most of the vector mesons could result from decays of higher excited meson states. In this context, it is worth while to study the Lund string model, which sheds some light on this problem. In a 1+1 dimensional world, there is no distinction between a string and a meson; the fragmentation of a $q\bar{q}$ pair might just as well be described as the decay of a heavy, short-lived meson (see Figure 16(a),(b)). Similary, we could say that a string decays first to massive substrings, which in turn decay to hadrons, or that the entire string decays directly to hadrons (Figure 16(c),(d)) — the two views are mathematically equivalent (26). The question "what are the primary hadrons?" becomes a matter of semantics. In a three-dimensional world, it is unfortunately not clear if the same bootstrap principle works: low-mass hadrons and clusters decay isotropically, whereas high-mass strings remember the direction of the quarks at their ends.

Interpretation of Meson Rates I: Strangeness Suppression and Spin Dependence

The most obvious feature of meson cross sections are the strong deviations from SU(6) symmetry among stable hadrons; differences persist among primary hadrons, at least if we restrict ourselves to the P and V meson nonets (column 1 of Table 4). The SU(6) breaking among primary hadrons is often summarized in terms of two phenomenological parameters: the strangeness suppression factor s/u describing the relative production rates of $s\bar{s}$ and $u\bar{u}$ quark pairs, and the fraction V/(V+P) of mesons produced in spin-1 states (neglecting nonets other than the pseudoscalars and vectors). In this parameterization, the production rate of a meson is given by the product of a weight for each of its quarks, a spin weight,

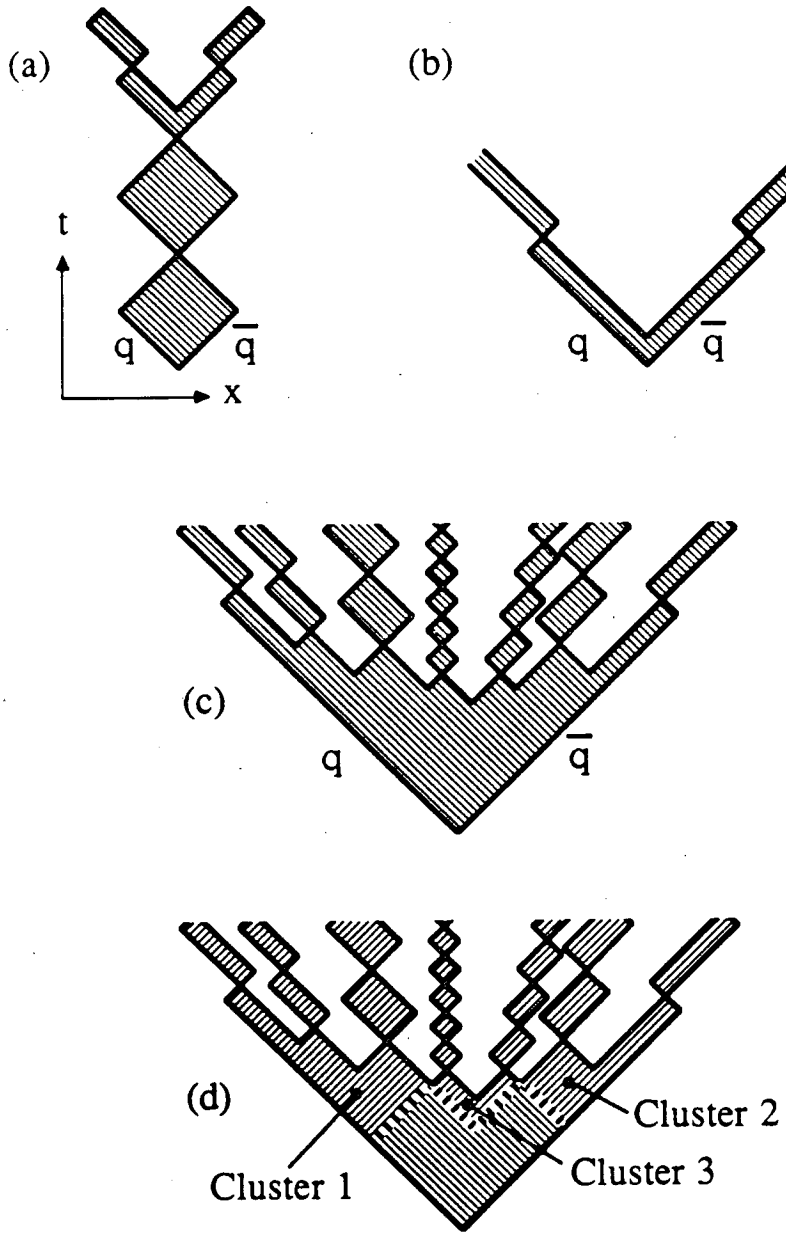

Figure 16 (a) Space-time diagram of a string describing propagation and decay of a meson in 1+1 dimension. (b) Two-meson decay of a string created in e^+e^- annihilation. (c) A long string, decaying directly into low-mass hadrons. (d) The same process, viewed as a decay into heavy clusters, followed by the decay of the clusters.

and (for neutrals) coefficients to describe mixing. Phenomenologically, a strangeness suppression s/u < 1 is motivated by the finite energy energy density in the string; in 1+1 dimension, the fermion production rate can be estimated to be $\sigma \sim \exp(-\pi m_q^2/\kappa)$, resulting in a strange-quark suppression of about 0.3 for typical values of (constituent) quark masses m_q and string tension κ (28). One can motivate a vector meson suppression in terms of the larger binding energy of pseudoscalars; since quark-pair production is always viewed as a quantum fluctuation, a pair has a better change of materializing if one of its quarks "knows" that it is going to fall into a deep binding potential (24).

Only experiment can decide if a description in terms of s/u and V/(V+P) is sensible and consistent. Conditions for consistency are

1) s/u determined from K,K* and π,ρ should agree with the values obtained from D_S and $D^{\pm,o}$ and from B_S and $B^{\pm,o}$ mesons. If V/(V+P) has a universal value, the same value of s/u should be obtained from comparison of K and π, of K* and ρ and of ϕ and K*.

2) s/u determined from baryons should agree with the value from mesons

3) s/u should not depend on $\sqrt{s}$, except for threshold effects.

The s/u and V/(V+P) parameters can be calculated using the rates of primary hadrons, as discussed in several reviews (94-96). From the rates given in Table 4, we find:

s/u	$= 0.29 \pm 0.06$	based on K* and ρ rates,
	$= 0.27 \pm 0.08$	based on K and π rates,
	$= 0.26 \pm 0.16$	based on ϕ and K* rates
V/(V+P)	$= 0.39 \pm 0.08$	based on ρ and π rates,
	$= 0.40 \pm 0.05$	based on K* and K rates.

These results are certainly self-consistent. We will see later that s/u $\approx$ 0.3 is also consistent with data on strange-baryon production; there, one finds s/u = 0.28 $\pm$ 0.23. Data on D_S production suffer from badly-known branching ratios, but are not (yet) inconsistent with

s/u ≈ 0.3. Other reviews arrive at similar values (94-96). Over the PETRA energy range, determinations of s/u (within the Lund model framework) give no indication of an energy dependence (Figure 17). Consistent results for s/u are also obtained for quark jets in deep-inelastic lepton-nucleon scattering with W > 10 GeV (97-101). Below W ≈ 5 GeV, s/u shows a threshold effect.

A potential problem is indicated in a comparison with ISR data on high-p_T particle production (102). In order to model the observed K/π ratio in a QCD-based hard-scattering model, s/u ≈ 0.55 is required, a value well above the range compatible with e^+e^- data. Since high-p_T particles are usually leading particles in jets, one can speculate about a z-dependence (or better, a rank-dependence) of s/u (103). There are good reasons why such a dependence could arise: leading particles differ from central hadrons in that one of their quarks is already present, whereas normally both result from vacuum fluctuations. It is not clear if a z-dependence of s/u can be constructed which is consistent with both the ISR data and the K/π data of Figure 11.

Parameters labeled 's/u' appear in many Monte Carlo models; however, their meaning often differs from the one discussed above. Especially in QCD cluster models, these parameters refer to the primary hadrons or clusters, and act in addition to kinematic constraints and phase-space weights. The resulting strangeness suppression among vector and pseudoscalar mesons may differ substantially from the input value. For example, QCD cluster models input s/u values in the 0.6 - 1.0 range in order to reproduce the observed kaon yields. In the Lund model, on the other hand, meson flavor composition is imposed entirely by the s/u and V/(V+P) parameters and one gets out (within a few %) whatever is put in.

We conclude this section with a discussion of the complete set of Lund-model flavor parameters. In addition to the s/u parameter, the model contains separate V/(V+P) parameters

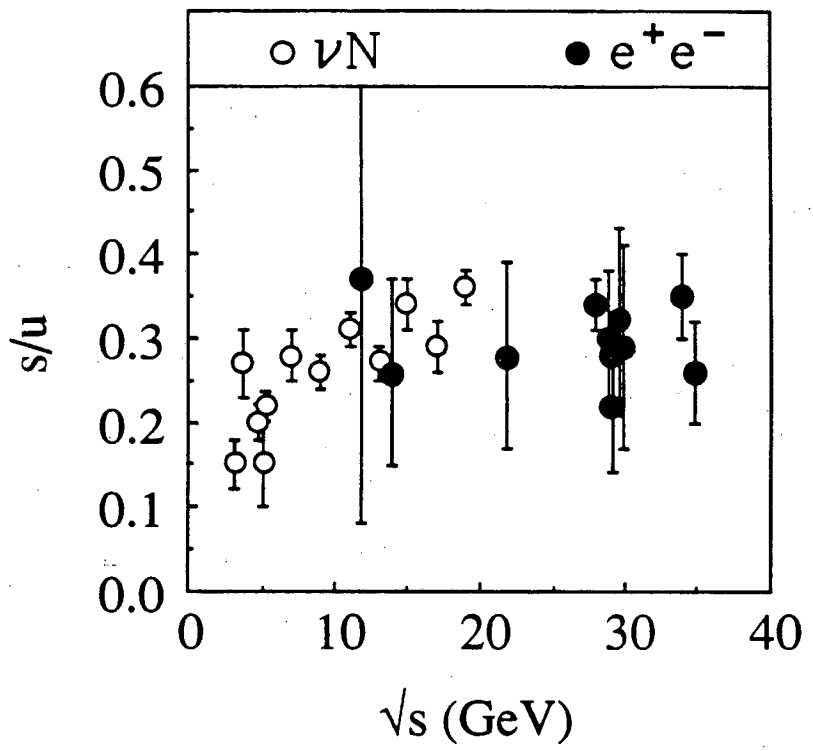

Figure 17 Compilation of values of the s/u strangeness suppression parameter measured in e^+e^- annihilation (34,43,46,104) and in quark jets in deep-inelastic lepton-nucleon scattering (97-101), as a function of the mass of the hadronic system ($\sqrt{s}$ or W). Some of the errors bars refer to statistical errors only; systematic errors are typically ±0.05 or more.

for nonstrange, strange, and charmed mesons as well as three major parameters governing baryon rates (to be discussed later). As pointed out earlier, these parameters are highly correlated and their determination is non-trivial. Besides the technique used above (which is more transparent, but not quite as precise), groups have used iterative global fits. Two of the most complete sets of results are shown in Table 5. The first set is used by the HRS group (41) for best description of their inclusive data; quoted errors correspond to the diagonal terms only. The second set is based on a fit to a compilation of average multiplicities (similar to the one given in Table 2, but not completely identical), and quoted errors include correlations between parameters (104).

Table 5: Lund-model flavor parameters

	Defaults (Vs. 6.3)	HRS	Global fit
s/u	0.30	0.34 ± 0.03	0.29 ± 0.02
(qq)/q	0.10	—	0.09 ± 0.01
$(qq)_{J=1}/(qq)_{J=0}$ (*)	0.05	—	0.05 ± 0.04
(us/ud)/(s/d)	0.40	0.87 ± 0.06	0.7 ± 0.3
$V/(V+P)_{u,d}$	0.50	0.54 ± 0.06	0.41 ± 0.05
$V/(V+P)_s$	0.60	0.66 ± 0.08	0.46 ± 0.05
$V/(V+P)_c$	0.75	1.0 ± 0.3	0.62 ± 0.08

(*) $(qq)_{J=1}/(qq)_{J=0}$ parameter does not include factor 3 from spin counting.

Interpretation of Meson Rates II: Mass Dependence

The parameterization discussed above suggests that the strangeness suppression occurs at the quark level. Given that the time scales for quark production and hadron formation are similar, one may wonder if cross sections are mainly dominated by hadron parameters rather than quark properties. Plots of hadron rates vs mass (Figure 3) support this picture to some extent: a simple exponential mass dependence describes rates over a range of almost four orders of magnitude, within factors of 3 or so. Closer inspection however shows that the exponential describing K,K* and K_2^* is suppressed compared to the exponential fit to the π,ρ and f_2 data. Nevertheless, a pure mass dependence of hadron rates is not ruled out, if conservation laws are properly taken into account. Production of a kaon, for example, is always accompanied by the production of another hadron with a mass around 500 MeV or more, whereas for nonstrange mesons the constraint of charge conservation can always be fulfilled by production of a pion. Similar arguments hold for baryon production.

In order explore if a pure mass dependence can explain the hadron composition in quark jets, the Lund model was modified accordingly by Buchanan and Chun (104). As a minimal input, they assume that the fragmentation function of Equation (5) does not only describe the z-dependence, but that its integral also gives the probability to produce a hadrom of mass m in the next breaking of the string. Basically, this means that the probability for a multiparticle final state is given by Equation (4), with identical coefficients $N_i \equiv N$ for all hadrons. Production of heavy hadrons increases the space-time area swept by the string and is suppressed; the suppression is enhanced if particles have to be pair-produced. Both rates and inclusive distributions are governed by only two parameters, compared to about a dozen in the normal Lund string model. Despite the minimal assumptions, the model reproduces experimental rates rather well (104), and its results are

virtually identical to those of the ordinary Lund model with its numerous parameters. At first, it seems surprising that baryon rates are correctly reproduced, given the strong suppression of baryon pair production due to the exponential area law (the increase in area is proportional to m^2). This suppression is however offset by the fact that there are many more baryon flavor and spin states than there are meson states. In fact, the model shows a tendency to overestimate decuplet baryon rates.

It is hard to judge how realistic such a model is – whereas a pure mass dependence may be natural in a 1+1 dimensional limit, one would expect that in 3+1 dimensions the coefficients N_i in Equation (4) contain overlap integrals between hadron and quark wavefunctions, and do depend on the hadron species. Nevertheless, the model demonstrates that hadron rates can be described by a simple hadron-mass dependence of the production matrix elements.

CHARMED HADRONS AND HEAVY QUARK FRAGMENTATION

It is generally assumed that the production of heavy (C or B) quarks in both the perturbative and the nonperturbative evolution is negligible compared to the 8/11 charm quarks per event produced at the primary vertex, plus the more than 2/11 charmed hadrons from B hadron decays at energies above the B threshold. The fragmentation of heavy quarks into heavy hadrons is characterized by a hard fragmentation function. Two components contribute to the hard fragmentation, compared to pion or kaon distributions: firstly, we consider only the leading hadron. Secondly, the confinement process ends after a shorter time, or correspondingly at a larger mass scale, and the heavy quark has less opportunity to feed energy into the color field. Detailed perturbative and nonperturbative models sustain this general argument, although the predictions concerning the exact mass dependence differ (106-109). Experimental results on heavy quark fragmentation have been summarized by

Bethke (110). The most precise data on charmed-hadron spectra come from experiments in the Upsilon energy range, and are well described by the string-model fragmentation functions (Figure 18).

Flavor Composition of Heavy Hadrons

In principle, the production rates of different flavors of charmed and bottom hadrons provide an excellent testing ground for hadronization models; for example, by comparison with light quarks it should be easy to determine if production rates are governed by quark-level suppression factors or essentially only by hadron masses. Unfortunately, no data exist on identified hadrons with b quarks, and data on charmed hadrons suffers from badly-known branching ratios of D_S and Λ_C. Assuming that a charm quark picks up u,d,s quarks and diquarks in the same proportions as found for light quarks, one expects about $\frac{8}{10}\left(\frac{2}{2+s/u}\right)\left(\frac{1}{1+qq/q}\right) \approx 0.65$ D^0, D^+ per event (including antiparticles) below B threshold, and about 0.75 above (with $\approx$ 1.15 c-quarks per b-quark decay). The experimental values of 0.57±0.08 and 0.52±0.09 (at 29 GeV and at 10 GeV, respectively, using the revised MARK III branching ratios (111)) indicate that $28 \pm 10\%$ and 45±10%, respectively, of the primary charmed quarks appear in D_S or in charmed baryons, compared to the naive expectation of about 20%. Direct measurements of D_S in the $\phi\pi$ decay mode exist, but cannot confirm the excess, since the branching ratio $B_{\phi\pi} \approx 3\%$ has not been independently determined; it derived *assuming* $s/u \approx 0.3$ for charmed mesons. Measurements of Λ_C production also suffer from poorly known branching ratios; data from ARGUS and CLEO translate into $qq/q \approx 0.30 \pm 0.12$ for charmed hadrons, compared to the usual value $qq/q \approx 0.1$. While it has been argued that the s/u or qq/q ratios may be different for charmed hadrons, neither of the QCD cluster models predicts a large increase; one finds effective s/u ratios between 0.33 (Caltech) and 0.40 (Webber), and charmed-baryon to meson ratios are

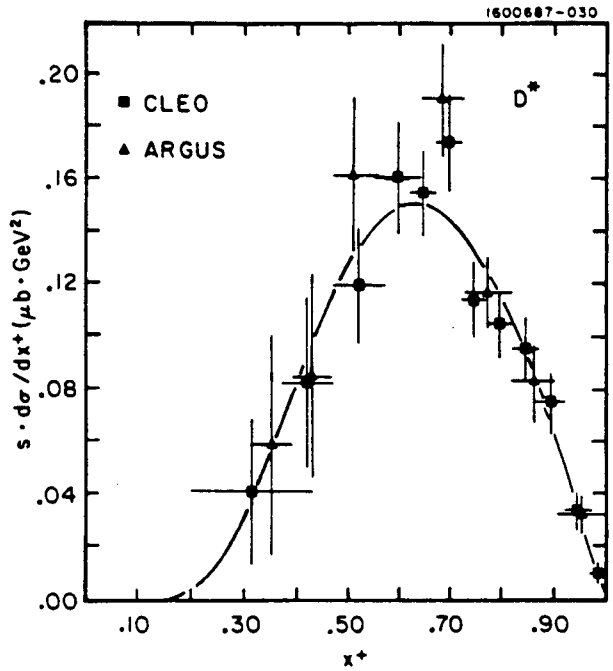

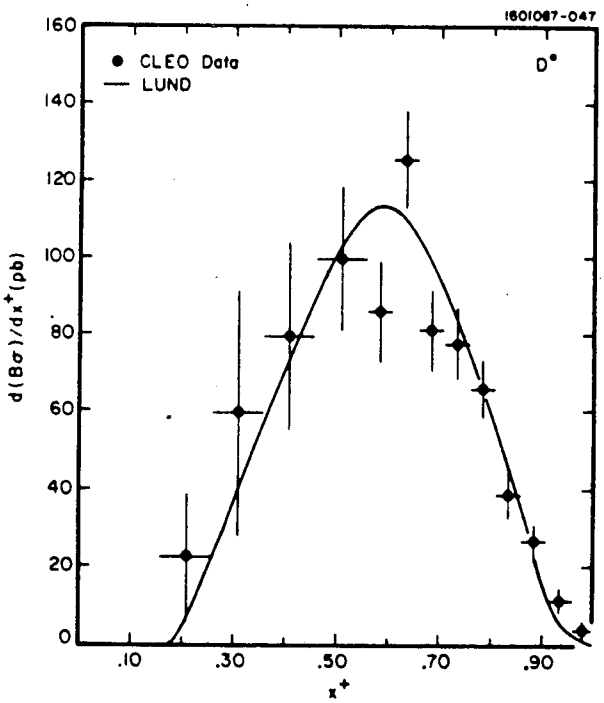

Figure 18 (a) $D^{\pm}$ cross section $s\, d\sigma/dx^{+}$ as a function of the light-cone variable $x^{+} = \frac{(E+p)}{(E+p)_{max}}$. (b) D^{o} cross sections $s\, d\sigma/dx^{+}$. CLEO and ARGUS data at $\sqrt{s} \approx 10$ GeV (50,63). The curves show Lund model results, with parameters optimized to fit the data (50).

actually smaller than in the Lund model. Unfortunately, present data are not precise enough for a definitive statement.

The ratio of vector to scalar mesons is predicted to differ for charmed and light hadrons (24), since deviations from spin counting are driven by the ratio of vector and pseudoscalar masses and should be small for the D*, D system. New CLEO data translate into V/(V+P) = 0.85 ± 0.20 for charm quarks, consistent with spin counting and 2 S.D. higher than vector fractions for light mesons. This has to be compared with the default $V/(V+P)_c$ = 0.75 in the Lund model, and with resulting effective $V/(V+P)_c \approx 0.6$ in the QCD models. A compilation of V/(V+P) values for different quark species is shown in Figure 19; the observed trends are not inconsistent with predictions $V/P = 3(M_V/M_P)^{-\alpha}$, based on string dynamics.

BARYON PRODUCTION

Ratios of baryon and meson production rates as well as the correlation between strangeness and spin of a baryon and its production cross section allow detailed tests of fragmentation phenomenology, beginning with the challenge to find a mechanism to explain the relatively large baryon rate observed in e^+e^- annihilation events.

Experimental results

At PEP and PETRA energies, about 0.6 protons per event are observed; including a similar number of neutrons (about 10% smaller due to isospin-symmetry violating electromagnetic effects), this means that about 1.1 baryons are produced per event, corresponding to more than 10% of the primary hadrons (see Table 4). The $\sqrt{s}$-dependence of mean multiplicities is steeper for baryons than for mesons; going from $\sqrt{s}$ = 10 GeV to 29 GeV about doubles most baryon rates, compared to a 30-50% increase in meson yields

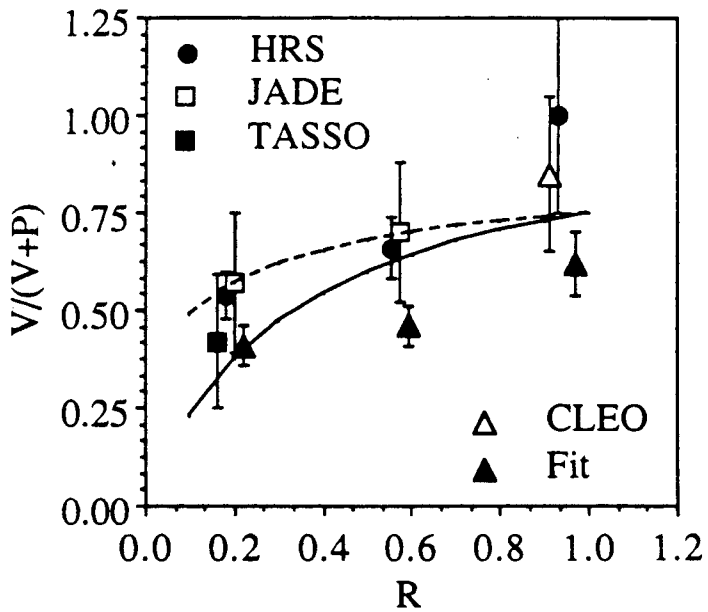

Figure 19 Fraction of vector mesons among primary mesons, as a function of the mass ratio R = m_P/m_V between pseudoscalar (P) and vector (V) mesons. Data: HRS (34), JADE (57), TASSO (60), CLEO (50) and global Lund-model fit (104). All analyses consider only vectors and pseudoscalars as primary mesons. Lines indicate analytical estimates, $V/P = 3(M_V/M_P)^{-\alpha}$, for $\alpha = 1$ (———) and $\alpha = 0.5$ (- - - - -).

(Figure 5). The extensive data on inclusive proton production has been presented earlier. Detailed results are also available on Λ production, see Figure 20. Comparison of Λ spectra at $\sqrt{s}$ = 10 GeV and at $\sqrt{s}$ = 29 GeV indicates a significant scale breaking, which is not unexpected (93), given that the mass of a baryon pair is non-negligible on a scale of 10 GeV. Of the other members of the octet, only the Ξ^- and, at 10 GeV, the Σ^o have been detected in high-energy e^+e^- annihilation. Of the decuplet, $\Sigma^{*\pm}$, Ξ^{*o} and Ω^- have been observed, the latter with considerable errors. The relative rates of different baryon species do not depend strongly on $\sqrt{s}$; the exception is the Ω^-, with a 20-fold increase between 10 and 29 GeV. Another related mystery shows up in the 29 GeV data: the observed Ω^- rate is larger than the upper limit for the Ξ^{*o} rate. One explanation is that the Ω^- at 29 GeV come from decays of hadrons with bottom quarks; another, that the PEP results on the Ω^- represent a (2 S.D.) statistical fluctuation.

In Figure 21, we display the strangeness dependence of baryon yields by forming cross section ratios for members of the same multiplet, such that the particle in the numerator has one additional strange quark compared to the particle in the denominator. Except for the already mentioned Ω^-/Ξ^{*o} data and for a Λ/p data point from CLEO, the observed ratios are consistent between experiments and are energy-independent. The Ξ^-/Λ data are atypical in that half or more of the Λ's are accounted for by decays of other hyperons. This effect is cancelled to some extent in the Λ/p ratio, since the p rate too is significantly increased by the same mechanism. The addition of one unit of strangeness is seen to cost about a factor 3 in cross section. Figure 22 shows ratios of decuplet and octet production rates for baryons with the same number of strange quarks. Even accounting for the increase in octet rates due to decuplet baryon decays, the ratios indicate a strong decuplet suppression compared to the 4:2 ratio expected from spin counting. The ARGUS group has also reported cross sections for the $\Lambda(1520)$, a J=3/2, L=1 state. It is produced at a similar rate as corre-

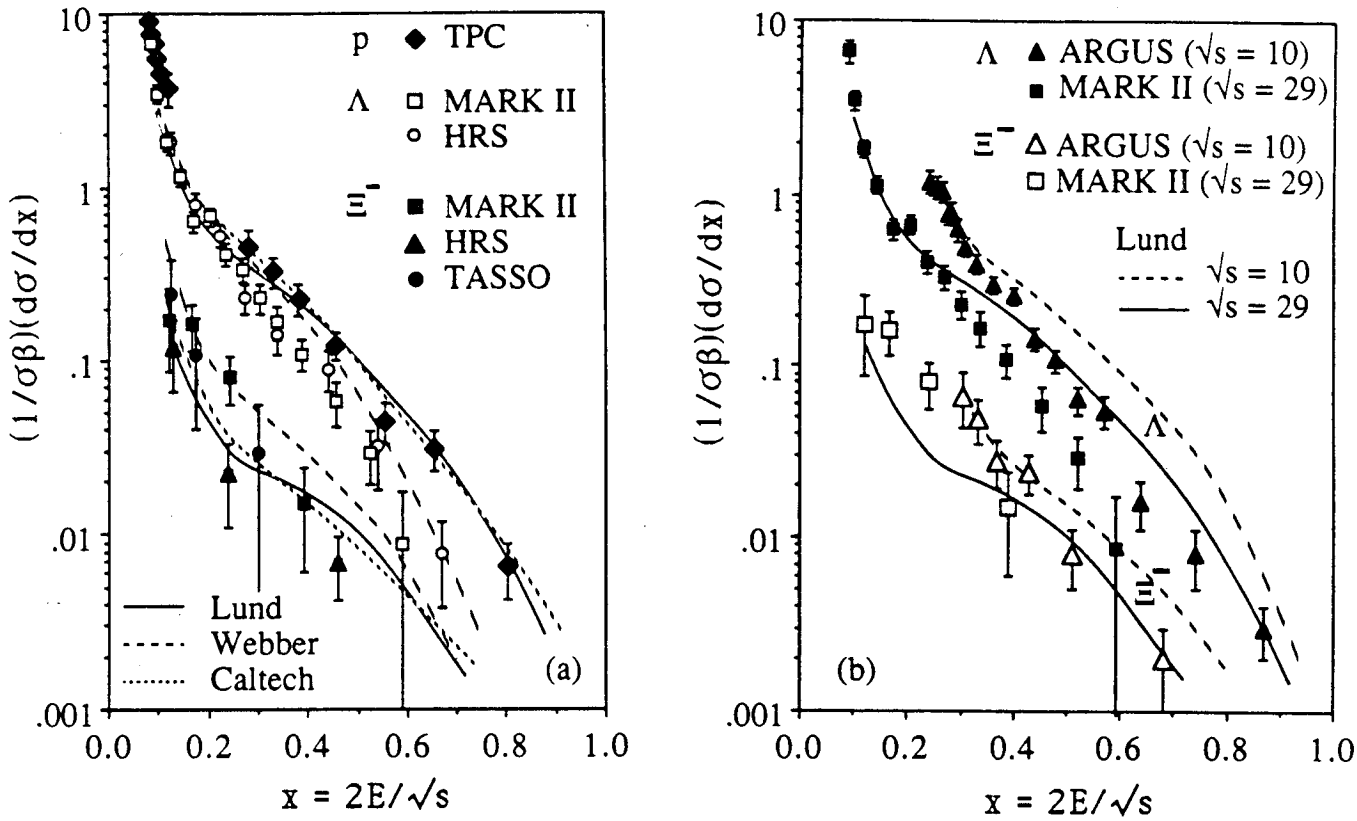

Figure 20 (a) Inclusive cross sections $(1/\sigma\beta)(d\sigma/dx)$ for production of J=1/2 baryons p, Λ, and Ξ^- in e^+e^- annihilation at $\sqrt{s} \approx 30$ GeV (HRS (79,82), MARK II (80,83), TASSO (84), TPC/2γ (36)). Lines indicate predictions of fragmentation models for Λ and Ξ^- (see Figure 5).

(b) Comparison of scaled Λ, and Ξ^- cross sections at $\sqrt{s} \approx 10$ GeV and at $\sqrt{s} = 29$ GeV (ARGUS (77), MARK II (80,83)). Lines indicate Lund model predictions for $\sqrt{s} = 10$ GeV (- - - - -) and $\sqrt{s} = 29$ GeV (———).

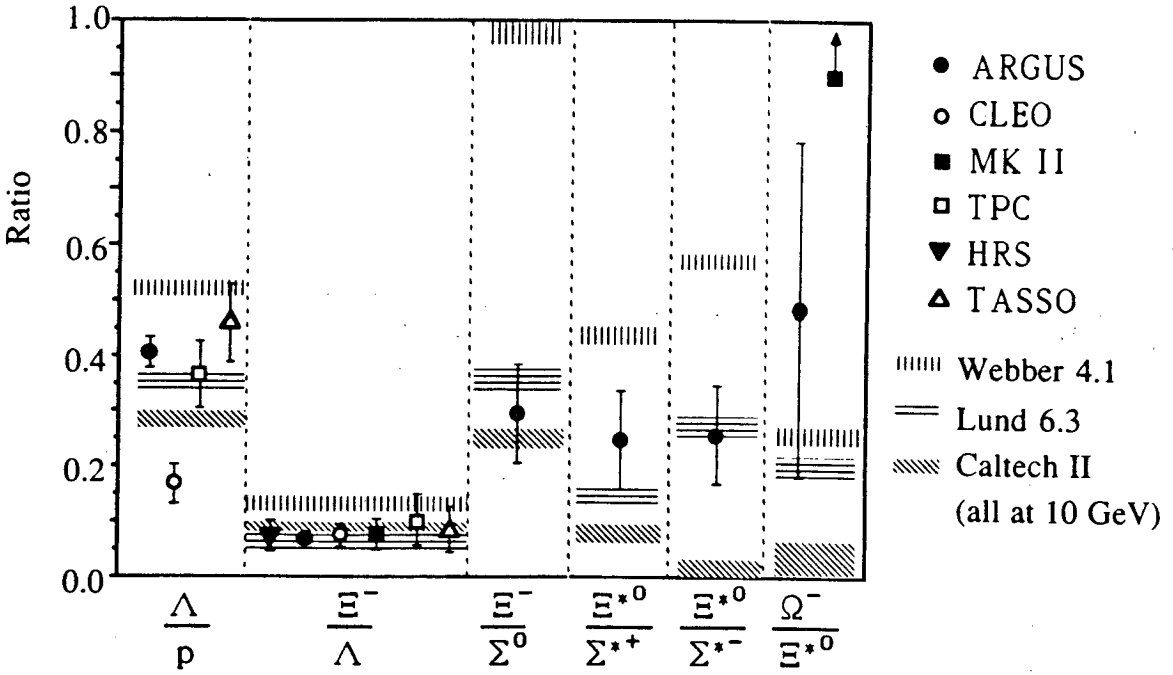

Figure 21 Strangeness suppression in baryon production. Shown are ratios of baryon cross sections for strangeness s+1 and s (s=0,1,2), for baryons in the same spin multiplet. Data from e^+e^- annihilation at $\sqrt{s} \approx 10$ GeV from ARGUS (77) and CLEO (33), and at $\sqrt{s} \approx 30$ GeV from HRS (79,82), MARK II (80,83,88), TASSO (35,46,84), and TPC (36,81,85). Shaded bands represent model predictions for $\sqrt{s} = 10$ GeV; the results for $\sqrt{s} \approx 30$ GeV are very similar.

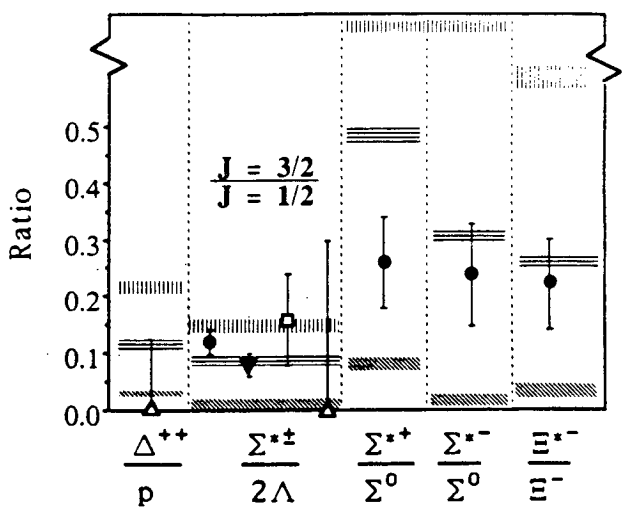

Figure 22 Ratios of cross sections for decuplet and octet baryons. Only baryons with same strangeness content are compared. See Figure 21 for legend and references.

sponding J=3/2, L=0 states, $\Lambda(1520)/\Sigma^* \approx 2$, and is suppressed compared to J=1/2, L=0 states, $\Lambda(1520)/\Lambda \approx 0.1$.

Phenomenology

Contrary to meson production (which can be seen as an extension of the perturbative preconfinement idea (17)), there is no completely obvious candidate for a mechanism to bring three quarks together. Baryon production by isotropic decay of heavy meson-like clusters (13) seems one of the most natural mechanisms, but fails in the explanation of baryon-antibaryon correlations (19,20). While other ideas have been proposed (112), most present models describe baryon production by means of diquark-antidiquark production in the (perturbative or non-perturbative) gluon field, followed by diquark-quark recombination (113-118). The interpretation of the true nature of a diquark ranges from "effectively pointlike objects" via "color fluctuations in a string" to "a bookkeeping trick". A very intuitive interpretation of the diquark mechanism is given in (115), and is implemented in the Lund model (116). In a color string, new quark pairs appear and disappear all the time as a result of quantum fluctuations. If a new pair has the right color, it screens the field and may eventually break the string (Figure 23(a)). A pair of the wrong color causes a change in field direction and color inside its space-time loop, but no energy is gained and the pair will disappear after a short time (Figure 23(b)). If, however, during that short time a quark pair of yet another color appears inside the first, then the three-quark groups on both sides may be in a color singlet state and the string is broken (Figure 23(c)). Effectively, the process can now be summarized as the production of a diquark-antidiquark pair. It is also possible that there occurs more than one string break inside the first loop, corresponding to a baryon-meson-baryon configuration (Figure 23(d)). Predictions of the qq/q ratio from the mechanism described above, though uncertain within factors 2 or more,

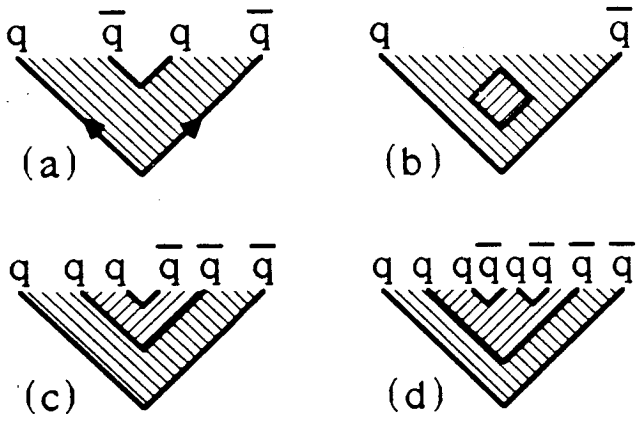

Figure 23 Model for baryon production in strings (115,116). (a) Screening of color field by new quark pair, resulting in meson production. (b) Wrong-color (non-screening) quark loop. (c) As (b), but with production of another (screening) pair inside the wrong-color quark loop. (d) As (c), but two pairs produced inside loop.

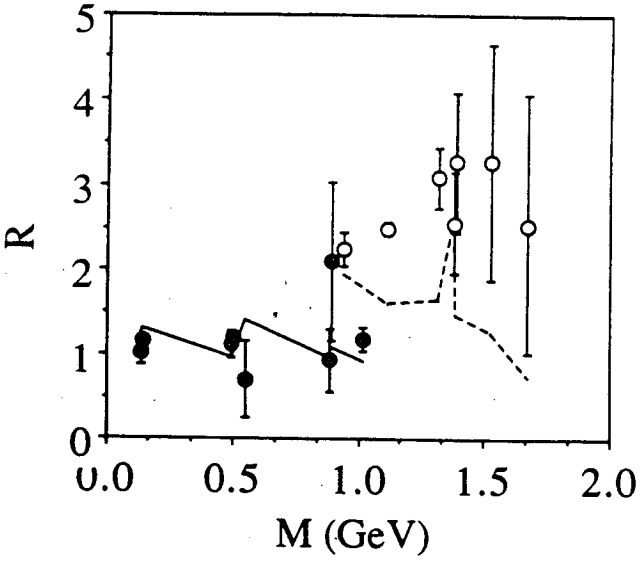

Figure 24 Ratio R of particle production rates in three-gluon decays of the Upsilon (1s) and in the nearby continuum, for mesons (•) and baryons (o), as a function of hadron mass. Data points combine ARGUS data (77), with statistical errors only, and CLEO (33) data. Solid and dashed lines represent Lund model predictions for mesons and baryons respectively.

fall in the right ballpark (115,116). Since QCD indicates a much lower mass of spin-0 diquarks compared to spin-1 diquarks, diquark models are generally characterized by a strong suppression of decuplet baryons. String models suggest an additional suppression of strange diquarks: (sd)/(ud) < s/u. The increased suppression is caused by the quadratic mass dependence of quark production rates (113,116).

In order to determine the rates at which different diquark states contribute, we use a simple analytical model assuming SU(6) symmetry broken by a strange-quark suppression s/u, and by independent suppression factors for different diquark SU(2) multiplets (87). Separate fits to the data around $\sqrt{s} \approx 10$ GeV and around $\sqrt{s} \approx 30$ GeV yield consistent parameters and good agreement ($\chi^2 < 1$/D.F.) except for the high-energy Ω^- data, which cannot be consistently described with this parameterization. If these Ω^- results are confirmed and are not caused by heavy-quark decays, diquark ideas will have to be abandoned or drastically modified.

Fixing $s/u = 0.30 \pm 0.03$, a joint fit to all baryon data yields the parameters

$$p_1 = \frac{(us)_0/(ud)_0}{s/u} = 0.49\ ^{+0.27}_{-0.20}$$

$$p_2 = (ud)_1/(ud)_0 = 0.03 \pm 0.03$$

$$p_3 = (us)_1/(ud)_0 = 0.012 \pm 0.004$$

$$p_4 = (ss)_1/(ud)_0 = 0.004 \pm 0.002.$$

The diquark index gives the spin. Note that $(uu)_0$, $(dd)_0$, $(ss)_0$ diquarks do not exist. As expected, spin-1 diquarks are suppressed by more than an order of magnitude compared to spin-0 diquarks. An extra suppression of strange diquarks is seen at the 2 S.D. level, but is less drastic than originally predicted (113). If s/u is allowed to vary, one finds $s/u = 0.28 \pm 0.23$; the large error is due to strong correlations between the parameters s/u and p_1.

Comparison with Models

In hadronization models, baryon quantum numbers (i.e. diquarks) can be generated in three places: during shower evolution by gluon splitting into diquarks, during the breaking of color strings, and in the decays of heavy clusters.

In the Lund hadronization model, baryon production is implemented using the string-breaking mechanism discussed in the previous section and illustrated in Figure 23. The rate of diquarks is determined by a parameter $qq/q \approx 0.1$. The diquark species is selected according to a parameterization similar to the one given above, except that rates factor into a flavor-dependent term (the extra suppression for strange diquarks) and a spin-dependent term (spin-1 suppression). Primary baryons are taken from the octet and decuplet. The strange-diquark suppression factors obtained in different analyses (see Table 5) are consistent with the value of p_1 given above; a similarly large spin-1 suppression is found. Total baryon multiplicities and flavor ratios are reasonably well reproduced (Figures 4,21,22), with the usual exception of the high-energy Ω^-. However, the z-dependence of baryon cross sections disagrees with data (Figures 5,11,20), possibly indicating that the fragmentation function f(z) (Equation 5) depends on the quantum numbers of a produced hadron, not just its mass.

In the Webber model, diquarks can be created both in the shower and in cluster decays. With the default parameters, diquark production in the shower is switched off. In cluster decays, the probability for any given two body decay into mesons or baryons is exclusively determined by the product of hadron-spin weights and phase space. No extra suppression of applied for strange quarks or for strange diquarks. The total baryon yield is largely a matter of phase space, but can be strongly influenced via the maximum cluster mass, above which clusters split into more clusters in a string-like fashion, rather than decaying into hadrons; this maximum mass W_{max} is usually set to 3.75 GeV. Since the baryon yield is

influenced by this ad-hoc parameter stronger than by any other parameter, the total baryon rate is not a genuine prediction of the model. The Webber model severely overestimates the rates for decuplet and strange baryons, since the spectrum of cluster masses around 2-3 GeV does not fall fast enough to effectively inhibit production of those heavier states. The data therefore indicate the need for real dynamics beyond phase space and spin counting.

In the Caltech II model baryon quantum numbers can be produced either in the decay of a heavy cluster (which is parameterized after low-energy data) or during the breaking of the string into clusters. In the cluster decay, a diquark suppression (uu)/u ≈ 0.5 - 0.7 and a strange diquark suppression (uu) : (us) : (ss) = 1 : 0.1 : 0.08 act in addition to phase space suppression and spin weights. More for the sake of economy rather than for a compelling reason, diquark rates in the string breaking are based on the same parameters. Comparison with data shows that the combination of parametric suppression and phase space is a little too effective — the Σ^*,Ξ^* and Ω^- rates are somewhat underpredicted. However, the scarcity of appropriate low-energy data to determine the cluster decay parameters allows quite a bit of adjustment.

PARTICLE COMPOSITION IN GLUON JETS

Attempts to identify differences in the particle composition between quark and gluon jets at PEP/PETRA have remained largely inconclusive. Much more revealing are comparisons between Υ decays into three gluons and $q\bar{q}$ events in the nearby continuum, as performed extensively by the ARGUS and CLEO groups (Figure 24). Mean meson multiplicities on and off resonance show only small differences, which at first is somewhat surprising, given that continuum events include initial strange and charmed quarks and might be expected to have a higher strangeness content. Monte Carlo studies however show that this effect is essentially cancelled by the large energy fraction carried away by charmed

hadrons, leaving less energy for production of extra $s\bar{s}$ pairs. In particular, no enhancement is observed in inclusive η rates, in contrast to predictions of the "leading isoscalar" model (119), according to which gluon jets contain leading glueballs mixing with isoscalars and enhancing η and η' rates.

A drastic difference in the baryon content of events on and off resonance has been known for a while, and is now firmly established: baryon multiplicities in $\Upsilon \rightarrow ggg$ decays are boosted by factors 2 to 3 over the nearby continuum (Figure 24). The effect is qualitatively predicted in the Lund string model (116). The two endpoints of the string representing a continuum event are quarks rather than diquarks, whereas ggg events start out as string loops without ends and therefore no place where baryon production is disfavored. Such a model predicts that the baryon to meson ratio in Υ decays should be close to that in the central region of high-energy $q\bar{q}$ events, away from the ends of the string. Data are consistent with this prediction (120) . However, the Lund model is not able to reproduce the Υ data quantitatively. QCD cluster models also predict a baryon enhancement caused by the increased rate of high-mass clusters in ggg events, and are able to reproduce the rise of the effect with baryon mass (121,122). It is presently not clear if the absence of an enhancement of heavy meson (ϕ) production is consistent with such an interpretation. Other qualitative explanations make use of the higher quark density in gluon-initiated showers, increasing the rate of three-body (qqq) recombination as compared to two-body ($q\bar{q}$) processes (123,124).

SUMMARY

Large amounts of data on inclusive hadron production have been accumulated over the last years at the PEP, PETRA, CESR and DORIS machines. Cross sections of identified charged stable hadrons are known with 5-10% errors, and have been studied as a function

of momentum, transverse momentum and rapidity with respect to the event axis. Production rates of the unstable members of the pseudoscalar nonet and of the vector meson nonet are known within 10-40%, and tensor mesons have been detected. Errors on cross sections of octet baryons range between 10 and 40%, and some decuplet states have been detected. The study of rates of mesons and baryons with charm and bottom quarks is still open, except for D* and D cross sections, which are reasonably well measured. Quark-flavor tagged cross sections would simplify the interpretation of data considerably.

Many features of the particle composition in jets can be described in terms of a combination of longitudinal phase space and particle decay kinematics, supplemented by a steep mass dependence of primary production rates.

In the phenomenology of hadron production in e^+e^- annihilation, significant progress has been made in the last ten years as far as the jet structure of the events and the flow of hadrons is concerned. String models and clusters models have taken us from a convenient parameterization of jet properties — the Feynman-Field model — to models emphasizing the physics of jets, based on extrapolation of results in perturbative and nonperturbative QCD. However, a consistent and coherent description of the hadron composition of jets is still missing. In the Lund string model, the generation of different hadron flavors is governed by free (albeit physically motivated and consistent) parameters in a fashion almost identical to the Feynman-Field model; taking SU(2) symmetry for granted, the number of free parameters is only slightly smaller than the number of well-measured particle species. QCD-based cluster models originally seemed like a big step forward, as far as simplicity and predictive power was concerned. However, these initial models failed to describe the particle spectra at large x, the correlations between baryons, and the flavor-dependence of baryon cross sections. While these and other problems have been dealt with by introducing special rules and additional parameters, the models have lost some of their initial appeal in

the process, and are still inferior to the string framework in their ability to reproduce experimental results.

A central point in this discussion is the question of the nature of the primary hadronic objects. Do all or most of the observed stable hadrons result from the isotropic decay of heavier hadrons? At which mass scale does the transition occur between systems oriented along the initial color-anticolor axis, and isotropically decaying objects? Is this a quantitative change, somewhat in the sense of a phase transisition, or simply a gradual loss of alignment? Experiments have so far been unable to answer these questions. The string picture comes closest in giving a phenomenological guideline, since (in 1+1 dimension) there is no fundamental distinction made between a string, a short-lived cluster, and a hadron. Unfortunately, the extension of these concepts into three dimensions is non-trivial.

Reflecting these problems, the phenomenological work on the nonperturbative aspects of particle production has slowed down, and the attentention of model builders has turned to improvements in the regime of perturbative QCD, and to applications in more complicated environments, such as hadronic interactions. Continuing work on the phenomenology of flavor composition of jets is largely based on the string framework. At the same time, however, new techniques in lattice QCD (105) are being developed, and may soon give new directions to both theory and experiment.

ACKNOWLEDGEMENT

This work was supported by the US Department of Energy under Contract No. DE-AC03-76SF00098, and by the Alfred P. Sloan Foundation. I want to thank my colleagues in the TPC/2γ collaboration for their help and advice in the preparation of this review.

Literature Cited

1. Drell, S. D. , Levy, D. J. , Yan, T.-M. , Phys. Rev. D1:1617 (1970)
2. Farrar, G. R. , Jackson, D. R. , Phys. Rev. Lett. 35:1416 (1975); Berger, E. L. , Z. Phys. C4:289 (1980); Matveev, V. A., et al, Nuovo Cimento Lett. 1:719 (1973); Brodsky, S., and Gunion, J., Phys. Rev. D17:848 (1978)
3. Bjorken, J. D., Proc. Int. Conf. on Physics in Collision, Stockholm, Sweden (1982), and FERMILAB-Conf-82/42-THY (1982)
4. Sjöstrand, T., LU TP 87-18, to be published in Int. J. Mod. Phys. A
5. Gottschalk, T. D., Calt-68-1075 (1987)
6. Webber, B. R., Ann. Rev. Nucl. Part. Sci. 1986, 36:253
7. Kramer, G. , Theory of Jets in Electron-Positron Annihilation. Berlin: Springer, (1984)
8. Konishi, K., Ukawa, A., Veneziano, G., Phys. Lett. 78B:243 (1978)
9. Basetto, A., Ciafaloni, C., Marchesini, G., Phys. Rep. 100:201 (1983);
10. Marchesini, G., Webber, B. R., Nucl. Phys. B238:1 (1984)
11. Azimov, Ya. I., et al, Z. Phys. C27:65 (1985)
12. Cohen-Tannoudij, G., Ochs, W., MPI-PAE/Pth 40-87 (1987)
13. Webber, B. R., Nucl. Phys. B238:492 (1984)
14. Fox, G. C., Wolfram, S., Nucl. Phys. B168:285 (1980)
15. Field, R. D., Wolfram, S., Nucl. Phys. B213:65 (1983)
16. Gottschalk, T. D., Nucl. Phys. B239:349 (1984)
17. Amati, D., Veneziano, G., Phys. Lett. 83B:87 (1979)
18. Gottschalk, T. D., Nucl. Phys. B239:325 (1984)
19. Aihara, H., et al, Phys. Rev. Lett. 57:3140 (1987)
20. Hofmann, W., Proc. of the Int. Symp. on Lepton and Photon Interactions, Hamburg, FRG, 1987; LBL-23922 (1987)
21. Gottschalk, T. D., Morris, D. A., Nucl. Phys. B288:729 (1987)
22. Artru, X., Phys. Rep. 97:147 (1983)
23. Casher, A., Neuberger, H., Nussinov, S., Phys. Rev. D20:179 (1979); D21:1966 (1980)
24. Andersson, B., et al, Phys. Rep. 97:31 (1983)
25. Azimov, Ya. I., et al, Phys. Lett. 165B:147 (1985)
26. Andersson, B., Gustafson, G., Soderberg, B., Z. Phys. C20:317 (1983)
27. Field, R. D., Feynman, R. P., Nucl. Phys. B136:1 (1978)
28. Brezin, E., Itzykson, C., Phys. Rev. D2:1191 (1970)

29. Baringer, P., et al, Phys. Rev. Lett. 56:1346 (1986)
30. Petersen, A., et al, SLAC-PUB 4290 (1987); Phys. Rev. D, in print
31. Matthiesen, U., Ph.D. Thesis, Dortmund, FRG (1987)
32. Orr, R. S., Proc. Int. Conf. on High Energy Physics, Berkeley (1986), p. 1166
33. Behrends, S., et al, Phys. Rev. D31: 2161 (1985)
34. Derrick, M., et al, Phys. Rev. D35:2639 (1987)
35. Althoff, M., et al, Z. Phys. C17:5 (1983); contribution submitted to the Int. Symp. on Lepton and Photon Interactions at High Energies, Kyoto, 1985
36. Aihara, H., et al, LBL-23737 (1988)
37. Behrend, H-J., et al, Z. Phys. 20: 207 (1983)
38. Bartel, W., et al, Z. Phys. C28:343 (1985)
39. Brandelik, R., et al, Phys. Lett. 108B:71 (1982)
40. Braunschweig, W., et al, Z. Phys. C33:13 (1986)
41. Aihara, H., et al, Z. Phys. C27:187 (1985)
42. Schellman, H., et al, Phys. Rev. D31:3013 (1985)
43. Bartel, W., et al, Z. Phys. C20:187 (1983)
44. Derrick, M., et al, Phys. Rev. D35:2639 (1987)
45. Berger, Ch., et al, Phys. Lett. 104B:79 (1981)
46. Althoff, M., et al, Z. Phys. C27:27 (1985)
47. Aihara, H., et al, Phys. Rev. Lett. 53:2378 (1984)
48. Abachi, S., et al, ANL-HEP-PR-87-106 (1987)
49. Wormser, G., SLAC-PUB-4466 (1987)
50. Bortoletto, D., et al, CLNS 87/105 (1987); subm. to Phys. Rev. D
51. Orr, R. S., Proc. Int. Conf. on High Energy Physics, Bari (1985), p.517
52. Derrick, M., et al, Phys. Rev. Lett. 53:1971 (1984); ANL-HEP-CP-86-75-mc (1986)
53. Albrecht, H., et al, Phys. Lett. 153B:343 (1985)
54. Abachi, S., et al, ANL-HEP-CP-86-71-mc (1986)
55. Derrick, M., et al, Phys. Rev. Lett. 54:2568 (1985)
56. Althoff, M., et al, Phys. Lett. 136B:130 (1984)
57. Bartel, W., et al, Phys. Lett. 145B:441 (1984)
58. Derrick, M., et al, Phys. Lett. 158B:519 (1985)
59. Schellman, H., et al, SLAC-PUB-3448 (1984)
60. Brandelik, R., et al, Phys. Lett. 117B:135 (1982)
61. Aihara, H., et al, Phys. Rev. Lett. 52:2201 (1984)

62. Abachi, S., et al, ANL-HEP-PR-87-89, (1987); subm. to Phys. Lett.
63 Albrecht, H., et al, Phys. Lett. 150B:235 (1985)
64. Yamamoto, H., et al, Phys. Rev. Lett 54:522 (1985)
65. Derrick, M., et al, Phys. Lett. 146B:261 (1984)
66. Bartel, W., et al, Phys. Lett. 146B:121 (1984)
67. Althoff, M., et al., Phys. Lett. 126B:493 (1983)
68. Aihara, H., et al, Phys. Rev. D34:1945 (1986)
69. Yelton, J. M., et al., Phys. Rev. Lett. 49:430 (1982)
70. Bartel, W., et al, Phys. Lett. 161B:197 (1985)
71. Low, E. H., et al, Phys. Lett. 183B:232 (1987)
72. Albrecht, H., et al, Phys. Lett. 146B:111 (1984)
73. Aihara, H., et al, Phys. Rev. Lett. 53: 2465 (1984)
74. Abachi, S., et al, Phys. Rev. Lett. 57:1990 (1986)
75. Albrecht, H., et al, Phys. Rev. Lett. 56:549 (1986); contribution to Int. Conf. on High Energy Physics, Berkeley, 1986
76. Bebek, C., et al, contribution to Int. Symp. on Lepton and Photon Interactions, Hamburg, 1987
77. Albrecht, H., et al., DESY 87-141 (1987)
78. Saxon, D. H., Proc. Int. Conf. on High Energy Physics, Bari (1985), p. 899
79. Baringer, P., et al, Phys. Rev. Lett. 56:1346 (1986)
80. de la Vaissiere, C., et al, Phys. Rev. Lett. 54: 2071 (1985); 55:263 (1985)
81. Aihara, H., et al, Phys. Rev. Lett. 54:274 (1985)
82. Abachi, S., et al, Phys. Rev. Lett. 58:2627 (1987)
83. Klein, S., et al, Phys. Rev. Lett. 58:644 (1987)
84. Althoff, M., et al, Phys. Lett. 130:340 (1983)
85. Barbaro-Galtieri, A., XV Int. Symp. on Multiparticle Dynamics, Lund 1984
86. Albrecht, H., et al., contribution to Int. Symp. on Lepton and Photon Interactions, Hamburg, 1987
87. Althoff, M., et al, Z. Phys. C26:181 (1984)
88. Klein, S., et al, Phys. Rev. Lett. 59:2412 (1987)
89. Bowcock, T., et al, Phys. Rev. Lett. 55:923 (1985)
90. Albrecht, H., et al, Phys. Lett. 157B:326 (1985)
91. Aguilar-Benitez, M., et al, Phys. Lett. 170B: 1 (1986)
92. Sjöstrand, T., Comm. Phys. Comm. 43:367 (1987)
93. Baier, R., Engels, J., and Satz, H., Nuovo Cimento 28A:455 (1975)
94. Wroblewski, A., Acta Phys. Pol. B16:379 (1985)

95. Malhotra, P. K., Orava, R., Z. Phys. C17:85 (1983)
96. Hofmann, W., Proc. of the Int. Symp. on Strangeness in Hadronic Matter, Bad Honnef, FRG (1987); LBL-23921 (1987)
97. Jones, G. T., et al, Z. Phys. C27:43 (1985)
98. Ammosov, V. et al, Phys. Lett. 93B:210 (1980)
99. Arneodo, M., et al, Z. Phys. C34:283 (1987), Phys. Lett. 145B:156 (1984)
100. Barker, N. J., et al, Phys. Rev. D34:1251 (1986)
102. Breakstone, A., et al, Phys. Lett. 135B:510 (1984)
103. Geist, W. M., Phys. Lett. 196B:251 (1987)
104. Buchanan, C. D., Chun, S. B. , Phys. Rev. Lett. 59:1997 (1987)
105. Eller, T., Pauli, H. C., Brodsky, S. J., Phys. Rev. D35:1493 (1987)
106. Bowler, M. G., Z. Phys. C11:169 (1981)
107. Kartvelishvili, V. G., et al, Phys. Lett. 78B:615 (1978)
108. Peterson, C., et al, Phys. Rev. D27:105 (1983)
109. Collins, P., Spiller, T., J. Phys. G11:1289 (1985)
110. Bethke, S., Z. Phys. C29: 175 (1985)
111. Adler, J., et al., SLAC-PUB-4291 (1987)
112. Schierholz, G., Teper, M., Z. Phys. C13:53 (1982)
113. Andersson, B., Gustafson, G., Sjöstrand, T., Nucl. Phys. B197:45 (1982)
114. Meyer, T., Z. Phys. C12:77 (1982)
115. Casher, A., Neuberger, H., Nussinov, S., Phys. Rev. D20:179 (1979)
116. Andersson, B., Gustafson, G., Sjöstrand, T., Physica Scripta 32:574 (1985)
117. Ilgenfritz, E. M., Kripfganz, J., Schiller, A., Acta Phys. Pol. B9, 881 (1978)
118. Bartl, B., Fraas, H., Majoretto, W., Phys. Rev. D26, 1061 (1982)
119. Petersen, C., Walsh, T. F., Phys. Lett. 91B:455 (1980)
120. Hofmann, W., Proc. XVI Int. Symp. on Multiparticel Dynamics, Kiryat Anavim (1985), p. 635
121. Field, R. D., Phys. Lett. 135B:203 (1984)
122. Ng, C.-K., Phys. Rev. D33: 3246 (1986)
123. Hofmann, W., Z. Phys. C10:351 (1981)
124. Dias de Deus, J., and Pimenta, M., Phys. Lett. 109B:89 (1982); Z. Phys. C19:365 (1983)

LAWRENCE BERKELEY LABORATORY
TECHNICAL INFORMATION DEPARTMENT
UNIVERSITY OF CALIFORNIA
BERKELEY, CALIFORNIA 94720